

Transforming Gaussian Processes With Normalizing Flows

Juan Maroñas^{*†}
PRHLT Research Center
Universitat Politècnica
de València

Oliver Hamelijnck[†]
Dept. of CS
University of Warwick
The Alan Turing Institute

Jeremias Knoblauch
Dept. of Statistics
University of Warwick
The Alan Turing Institute

Theodoros Damoulas
Depts. of CS & Statistics
University of Warwick
The Alan Turing Institute

Abstract

Gaussian Processes (GPs) can be used as flexible, non-parametric function priors. Inspired by the growing body of work on Normalizing Flows, we enlarge this class of priors through a parametric invertible transformation that can be made input-dependent. Doing so also allows us to encode interpretable prior knowledge (e.g., boundedness constraints). We derive a variational approximation to the resulting Bayesian inference problem, which is as fast as stochastic variational GP regression (Hensman et al., 2013; Dezfouli and Bonilla, 2015). This makes the model a computationally efficient alternative to other hierarchical extensions of GP priors (Lázaro-Gredilla, 2012; Damianou and Lawrence, 2013). The resulting algorithm’s computational and inferential performance is excellent, and we demonstrate this on a range of data sets. For example, even with only 5 inducing points and an input-dependent flow, our method is consistently competitive with a standard sparse GP fitted using 100 inducing points.

gether, these features have made GPs uniquely attractive for modeling natural phenomena in molecular biology (Einstein, 1905), physics (Uhlenbeck and Ornstein, 1930), and spatial statistics (Kriging, 1951).

Within Machine Learning, GPs are most commonly used as non-parametric Bayesian prior beliefs over functions, an idea dating back to O’Hagan (1978) and significantly expanded by Williams and Rasmussen (1996). Though GP priors can describe many functions, an ongoing line of work has constructed ever more expressive function priors at the expense of computational complexity (Snelson et al., 2003; Damianou and Lawrence, 2013; Wilson and Ghahramani, 2010; Lázaro-Gredilla, 2012; Garnelo et al., 2018). For instance, the work of Damianou and Lawrence (2013) and Lázaro-Gredilla (2012) considers layered compositions of GPs. While these priors are more expressive than single GPs, this comes at a price: For example, in the Deep GP (DGP) inference algorithm of Salimbeni and Deisenroth (2017), computations are $\mathcal{O}(NM^2 \cdot K + M^3 \cdot K)$, where N is the number of observations, $M \ll N$ the number of inducing points and K the total number of GPs (dozens per layer in the work of Salimbeni and Deisenroth, 2017).

The current paper produces a method capable of largely eliminating this trade-off between the expressivity and computational complexity of function priors: We present a simple yet powerful way of enlarging the class of GP priors without substantially increasing computational cost. Building on Wilson and Ghahramani (2010) and Wauthier and Jordan (2010), we apply parametric and invertible transformations (aka Normalizing Flows (Rezende and Mohamed, 2015)) to a GP—yielding a Transformed GP (TGP). In contrast to previous approaches however, the TGP also allows for Bayesian, input-dependent transformations. The TGP is more expressive than a GP, and can encode additional prior knowledge about the latent function (e.g., boundedness constraints). With a sparse variational inference scheme, the TGP’s run time is $\mathcal{O}(NM^2 + M^3)$ —virtually identical to that of stan-

1 Introduction

Gaussian Processes (GPs) are perhaps the most well-known stochastic processes. Their popularity derives from their two most important features: Not only are they infinite-dimensional generalizations of the multivariate normal distribution, but they also inherit numerous convenient properties from it. Most importantly, like its finite-dimensional counterpart, the GP is closed under marginalization and conditioning. To-

Preliminary work. Under review. ^{*}Work started while at an internship at the Alan Turing Institute. [†]Indicates equal contribution. Order decided using `numpy.random.randint(2)`

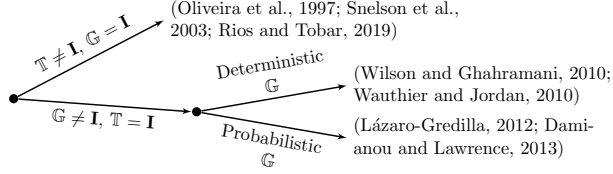


Figure 1: A simplified categorisation of some of the literature on transforming GPS.

dard sparse variational GP (SVGP) regression (Hensman et al., 2013). Further, the TGP outperforms the SVGP using only a fraction of its inducing points and produces test performances comparable to a multi-layer DGP.

While this is not a focus of the current paper, our inference scheme can also easily incorporate transformations of the data. This means we also provide a faster approximation to a number of previous models, including the Warped Gaussian Process (Snelson et al., 2003; Rios and Tobar, 2019).

2 Motivation

Existing literature uses invertible transformations within GPS either on the prior or the likelihood. For observations (\mathbf{X}, \mathbf{Y}) and invertible mappings \mathbb{G}, \mathbb{T} , a generative model unifying both approaches is

$$\left. \begin{aligned} \mathbf{f}_0 &\sim \text{GP}(\mu(\cdot), C(\cdot, \mathbf{X})); \quad \mathbf{f}_K = \mathbb{G}(\mathbf{f}_0) \\ \mathbb{T}(\mathbf{Y}) &= \mathbf{f}_K + \epsilon; \quad \epsilon \stackrel{iid}{\sim} \mathcal{N}(0, \Sigma). \end{aligned} \right\} \quad (1)$$

Denoting \mathbf{I} as the identity function, this recovers standard GP regression for $\mathbb{G} = \mathbb{T} = \mathbf{I}$. Similarly, setting $\mathbb{T} \neq \mathbf{I}, \mathbb{G} = \mathbf{I}$ / $\mathbb{G} \neq \mathbf{I}, \mathbb{T} = \mathbf{I}$ amounts to transforming only the likelihood / prior. Clearly, it is also possible to incorporate additional Bayesian priors about \mathbb{G} and \mathbb{T} . In this case, the transformation itself becomes probabilistic. Fig. 1 illustrates this categorization.

2.1 Related work

The arguable more popular subcase of Eq. (1) is applied to the likelihood ($\mathbb{T} \neq \mathbf{I}, \mathbb{G} = \mathbf{I}$). The methods resulting from this strategy are well-studied in spatial statistics, and also known as Trans-kriging models (Diggle and Ribeiro, 2007). The earliest work is based on exponential transforms such as the Box-Cox (Box and Cox, 1964), but transformations soon took various other forms, including the Tukey transform (Tukey, 1977), hyperbolic transformations (Tsai et al., 2017), and the Sinh-Archsinh transforms (Jones and Pewsey, 2009). Transformation parameters can be estimated (Snelson et al., 2003) or integrated out via Bayes’ rule

(Oliveira et al., 1997; Muré, 2018). In essence, transforming the likelihood is an attempt at Gaussianization (Chen and Gopinath, 2000; Meng et al., 2020): One hopes that \mathbb{T} makes $\mathbb{T}(\mathbf{Y}) = \mathbf{Z}$ into a standard GP with additive noise (Lin and Joseph, 2019). Note that whenever \mathbb{T} is non-linear, this implies that $\mathbf{Y} = \mathbb{T}^{-1}(\mathbf{Z})$ is non-Gaussian with non-additive noise. Thus, one can also see these transformations as aiming to fix model misspecification. This means that unlike other approaches towards robustifying GPS (see e.g. Jylänki et al., 2011; Hartmann and Vanhatalo, 2019; Knoblauch, 2019), transformations of the likelihood make sense *only* if one has sufficient domain knowledge to locate the source of misspecification.

On the other hand, transformations of the prior ($\mathbb{G} \neq \mathbf{I}, \mathbb{T} = \mathbf{I}$) have *no* implications for the likelihood model or error structure. Further—and unlike transformations of the likelihoods—they are applicable for discrete-valued data, too. This makes them more compatible with black box models—and so more attractive to the Machine Learning community: This does not mean that \mathbb{G} cannot incorporate domain knowledge however—and we exploit this on two applications where we force the function prior to be non-negative.

These advantages have made the literature on transforming the GP prior an active research area. Some of its most prolific outcomes include Wilson and Ghahramani (2010) as well as the work of Wauthier and Jordan (2010) and Murray et al. (2009). In all three papers, the parameterizations of the transforms are deterministic. More recently, this was superseded by a probabilistic treatment (e.g. Monterrubio-Gómez et al., 2020). Deep GPS (Damianou and Lawrence, 2013) and Warped GPS (Lázaro-Gredilla, 2012) are perhaps the most prominent examples, and transform a base GP with a layered hierarchy of other GPS. A different line of work transforms the prior via the input \mathbf{X} (see Calandra et al., 2016; Wilson et al., 2016), which induces non-stationarity relative to the original observation space without affecting the conditional Gaussianity of \mathbf{Y} .

2.2 Computation

Since the posterior of a standard GP regression ($\mathbb{G} = \mathbb{T} = \mathbf{I}$) has closed form, it is important to determine how much $\mathbb{G} \neq \mathbf{I}$ or $\mathbb{T} \neq \mathbf{I}$ complicates computations.

When the likelihood is transformed ($\mathbb{T} \neq \mathbf{I}, \mathbb{G} = \mathbf{I}$), marginal likelihoods often have closed forms (see e.g. Snelson et al., 2003). However, predictions need an explicit computation of the inverse \mathbb{T}^{-1} .

This leaves two options, both with considerable drawbacks: One can use approximation algorithms (e.g., Newton-Raphson) to approximate \mathbb{T}^{-1} , or one can

constrain \mathbb{T} to produce closed forms (see e.g. Rios and Tobar, 2019). The former bloats the computation and is sensitive to initial conditions, the latter constrains the model’s flexibility.

When the prior is transformed ($\mathbb{T} = \mathbf{I}$, $\mathbb{G} \neq \mathbf{I}$), the inverse \mathbb{G}^{-1} does *not* have to be computed explicitly. Such methods pose other challenges however: Their marginal likelihoods will not have closed form. In prior work, this has often resulted in rather coarse approximate inference. For example, Wilson and Ghahramani (2010) and Wauthier and Jordan (2010) set $\mathbb{G} \neq \mathbf{I}$ to obtain non-Gaussian marginals, but are forced to use Laplace approximations for inference.

The problem is compounded if \mathbb{G} itself is probabilistic, as is the case for Deep GPs (DGPs). To address this issue, sparse GP priors and Variational Inference (VI) are typically used. For instance, Damianou and Lawrence (2013); Lázaro-Gredilla (2012) use a mean-field normal family. This is extended by Salimbeni and Deisenroth (2017) to capture uncertainty across layers. Unfortunately, both approximations have drawbacks, leading to recent work advocating for structured variational families instead (Ustyuzhaninov et al., 2020). This appears to produce better inferences, but also significantly increase the computational overhead.

2.3 Our Contribution

We design a Bayesian method that can match the performance of Deep GPs at a fraction of the computational cost. To achieve this, we consider Bayesian Neural Networks (NNS) as input-dependent parametric transforms. We then derive a sparse variational approximation extending the ideas of Titsias (2009); Hensman et al. (2013) and Dezfouli and Bonilla (2015).

Our approximation is also the first scalable variational method for the methods of Wilson and Ghahramani (2010); Wauthier and Jordan (2010). Further, our inference algorithm is applicable even if one also transforms the likelihood ($\mathbb{G} \neq \mathbf{I}$, $\mathbb{T} \neq \mathbf{I}$). This means that it can easily be adapted to incorporate domain knowledge via \mathbb{G} (and \mathbb{T}), and we show this on two examples.

3 Model Description

Given N input-output tuples $\{(\mathbf{X}^{(i)}, \mathbf{Y}^{(i)})\}_{i=1}^N$, we arrange them into matrices $\mathbf{X} \in \mathbb{R}^{N \times D_x}$ and $\mathbf{Y} \in \mathbb{R}^{N \times D_y}$. Throughout, our goal is the Bayesian learning over a set of functions $\mathcal{F} = \{f : \mathcal{X} \rightarrow \mathcal{Y}\}$. To this end, we place a prior distribution over a subset of possible functions \mathcal{F} . Given a GP specified via its mean and covariance functions $\mu(\cdot)$, $C_\nu(\cdot, \cdot)$, we achieve this by additionally transforming it with K invert-

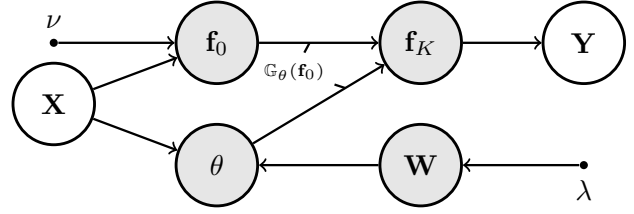


Figure 2: Plate diagram of the TGP with Bayesian input-dependent flows. We use transformations \mathbb{G}_θ with input-dependent (function-valued) parameters $\theta = \theta(\mathbf{X}, \mathbf{W})$ to transform a base GP \mathbf{f}_0 with kernel hyperparameters ν into a more expressive prior \mathbf{f}_K about the functional relationship between \mathbf{X} and \mathbf{Y} . In practice, \mathbf{W} will be weights of a Neural Network (NN) with a Bayesian prior depending on hyperparameters λ .

ible parametric transformations $\{\mathbb{G}_{\theta_k}\}_{k=0}^{K-1}$. More precisely, we define for all $k = 0, \dots, K-1$ the functions $\mathbb{G}_{\theta_k} : \mathcal{F} \rightarrow \mathcal{F}$ as the individual transformations, $\mathbb{G}_\theta = \mathbb{G}_{\theta_0} \circ \mathbb{G}_{\theta_1} \circ \dots \circ \mathbb{G}_{\theta_{K-1}}$ as their composition and $\theta = \{\theta_0, \theta_1, \dots, \theta_{K-1}\}$ as the parameterization of this composition. Transformations of this kind have recently been popularized in a different context as flows (Rezende and Mohamed, 2015). While our model applies for $\theta \in \mathbb{R}^p$, it also accommodates the case of function-valued (i.e. input-dependent) parameters $\theta : \mathcal{X} \rightarrow \mathbb{R}^p$ such as Neural Networks (NNS).

3.1 The Transformed Gaussian Process (TGP)

Taking $\mathbf{f}_0 \sim \text{GP}(\mu(\mathbf{X}), C_\nu(\mathbf{X}, \cdot))$ as a sample from the base GP, we then define the TGP as $\mathbf{f}_K = \mathbb{G}_\theta(\mathbf{f}_0)$. For simplicity, the current paper restricts attention to element-wise mappings. Because such mappings produce diagonal Jacobians, they only affect the marginals of the GP, so that for any fixed $\mathbf{X}' \in \mathcal{X}$, $\mathbf{f}_K(\mathbf{X}') = \mathbb{G}_\theta(\mathbf{f}_0(\mathbf{X}'))$. Thus, we will often refer to them as *diagonal/marginal* transformations/flows. Note that the resulting TGP \mathbf{f}_K can be seen as an input-dependent generalization of the Gaussian Copula Process discussed in Wilson and Ghahramani (2010).

3.2 Input-dependent Flows

A simple example for a marginal flow is given by stacking K SAL flows (Rios and Tobar, 2019):

$$\left. \begin{aligned} \mathbf{f}_1 &= d_1 \cdot \sinh(b_1 \cdot \text{arcsinh}(\mathbf{f}_0) - a_1) + c_1 \\ &\dots \\ \mathbf{f}_K &= d_K \cdot \sinh(b_K \cdot \text{arcsinh}(\mathbf{f}_{K-1}) - a_K) + c_K \end{aligned} \right\} (2)$$

In this example, \mathbb{G}_θ is not input-dependent and $\theta_{j-1} = \{a_j, b_j, c_j, d_j\}$. Fig. 3 illustrates the effect of such a

transform on a base GP for $K = 3$. We could make the transformation input-dependent however: The only thing required is a reparameterization. In particular, one only has to replace the scalar parameters a_j , b_j , c_j , and d_j with the function-valued parameters $\alpha_j, \beta_j, \gamma_j, \delta_j : \mathcal{X} \rightarrow \mathbb{R}$.

We achieve this via Neural Networks (NNS) with L layers so that for any fixed $\mathbf{X}' \in \mathcal{X}$, the transformation's parameters are $\{\alpha_j(\mathbf{X}'), \beta_j(\mathbf{X}'), \gamma_j(\mathbf{X}'), \delta_j(\mathbf{X}')\}_{j=0}^{K-1}$. Thus, if the NN's weights $\{\mathbf{W}^l\}_{l=1}^L$ are fitted without accounting for parameter uncertainty, $\boldsymbol{\theta} = \{\mathbf{W}^l\}_{l=1}^L$.

3.3 Bayesian Priors on Flows

However, we find that a Bayesian treatment of $\{\mathbf{W}^l\}_{l=1}^L$ significantly improves test set performance. This is hardly surprising: Input-dependent flows in the form of NNS introduce a considerable number of additional hyperparameters, making a naive implementation prone to over-fitting. By placing a Bayesian prior $p(\mathbf{W})$ on the network weights $\mathbf{W} = \{\mathbf{W}^l\}_{l=1}^L$, we effectively regularize the network weights and avoid this issue. This means that we integrate over $\{\mathbf{W}^l\}_{l=1}^L$, accounting for uncertainty in $\boldsymbol{\theta}$.

Though the prior could be chosen arbitrarily, we consider the fully factorized normal prior $p_\lambda(\mathbf{W}) = \mathcal{N}(\mathbf{W}; 0, \lambda^{-1} I_{|\mathbf{W}| \times |\mathbf{W}|})$ throughout the paper. The corresponding graphical model is given in Fig. 2, and the generative process is

$$\begin{aligned} \mathbf{f}_0 | \mathbf{X} &\sim \text{GP}(\mu(\mathbf{X}), C_\nu(\mathbf{X}, \cdot)) & \mathbf{W} &\sim p_\lambda(\mathbf{W}) \\ \boldsymbol{\theta}(\mathbf{X}, \mathbf{W}) &= \text{NN}(\mathbf{X}, \mathbf{W}) & \mathbf{f}_K | \boldsymbol{\theta}, \mathbf{X}, \mathbf{W} &= \mathbb{G}_{\boldsymbol{\theta}(\mathbf{X}, \mathbf{W})}(\mathbf{f}_0) \end{aligned}$$

Unlike in previous work (e.g. Wilson and Ghahramani, 2010), we not only quantify uncertainty about the parameter $\boldsymbol{\theta}$, but also make it an input-dependent function.

3.4 Induced Distributions

By virtue of an iterated application of the change of variable formula and the inverse function theorem (see e.g. Rezende and Mohamed, 2015), the probability distributions induced by our transformations are given by:

$$p(\mathbf{f}_K | \mathbb{G}, \mathbf{X}) = p(\mathbf{f}_0 | \mathbf{X}) \prod_{k=0}^{K-1} \left| \frac{\partial \mathbb{G}_{\boldsymbol{\theta}_k}(\mathbf{f}_k)}{\partial \mathbf{f}_k} \right|^{-1}.$$

By using a marginal flow, Sklar's theorem (Sklar, 1959) implies that the dependencies in $p(\mathbf{f}_0)$ and $p(\mathbf{f}_K)$ are driven by the same Copula—the GP in our case. Though the copula is the same, \mathbf{f}_K will generally have non-Gaussian marginals (see Fig. 3). While the current paper restricts attention to diagonal mappings for

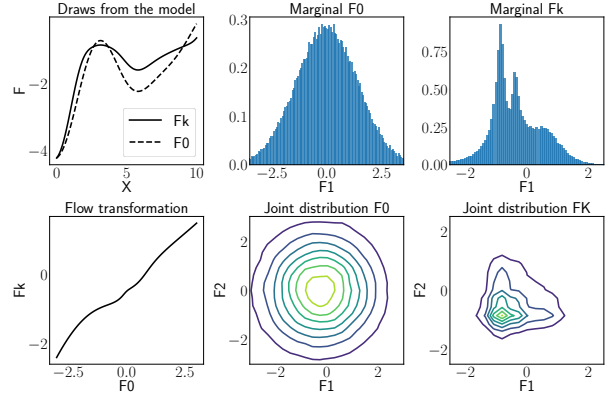


Figure 3: Flow constructed as in Eq. (2) with $K = 3$.

simplicity, the presented derivations and methods may be extended to non-diagonal transformations such as those in Rios (2020). In practical terms, non-diagonal transformations could be used to model arbitrary copulas and correlation structures; and we elaborate on this version of the model in App. A. Whether $\mathbb{G}_{\boldsymbol{\theta}}$ is a diagonal or non-diagonal transformation, \mathbf{f}_K is a valid stochastic process (and thus a valid function prior) by simple arguments (e.g. Rios, 2020).

4 Inference

Performing inference for the Transformed Gaussian Process (TGP) is generally intractable. Thus, we derive an efficient sparse variational approximation which is amenable to stochastic optimization (Hensman et al., 2013), utilizes inducing points through sparse GP priors (Titsias, 2009) and works with arbitrary likelihoods (Hensman et al., 2015; Dezfouli and Bonilla, 2015). An important part of this is a careful choice of the variational posterior, which eliminates the need to compute Jacobians or the inverse forms of $\mathbb{G}_{\boldsymbol{\theta}}$ altogether, yielding a drastic speedup. As a result, our inference algorithm is of order $\mathcal{O}(NM^2 + M^3)$ (for $M \ll N$) and parameters can be set via stochastic optimization. This makes our method particularly suitable for large-scale applications—and much faster than previous approaches: For example, the case of deterministic parametric transformations presented by Wauthier and Jordan (2010) and Wilson and Ghahramani (2010) relies on $\mathcal{O}(N^3)$ Laplace approximations. Similarly, the approximations for the case of hierarchical probabilistic transformations presented in Salimbeni and Deisenroth (2017) are of order $\mathcal{O}(NM^2 \cdot K + M^3 \cdot K)$, where K is the number of GPs inside the Deep GP (dozens per layer in the work of Salimbeni and Deisenroth, 2017).

4.1 Sparse Variational Objective

Variational methods frame inference as optimization by minimizing the Kullback-Leibler divergence (KL) between approximate and true posterior (Blei et al., 2017). It can also be interpreted as constrained finite-dimensional version of the infinite-dimensional variational problem characterizing the exact Bayesian posterior (Knoblauch et al., 2019). Rewriting this minimization as maximization, it becomes an Evidence Lower Bound (ELBO) (Bishop, 2006).

Sparse GPs augment the prior with M inducing points $\mathbf{u}_0 \in \mathbb{R}^M$ at locations $\mathbf{Z} \in \mathbb{R}^{M \times D}$, typically with $M < N$. These points act as ‘pseudo-observations’ and allow low rank approximations to the GP prior that circumvent the cubic costs traditionally associated with GP inference (Quiñonero Candela and Rasmussen, 2005; Williams and Seeger, 2001).

Taking the inducing points into account, the sparsified and transformed prior of the TGP is given by

$$p(\mathbf{f}_K, \mathbf{u}_K) = \underbrace{p(\mathbf{f}_0 | \mathbf{u}_0) \mathbf{J}_{\mathbf{f}_K}}_{=p(\mathbf{f}_K | \mathbf{u}_K)} \underbrace{p(\mathbf{u}_0) \mathbf{J}_{\mathbf{u}_K}}_{=p(\mathbf{u}_K)}, \quad (3)$$

where $p(\mathbf{u}_0)$ is a GP prior of the same form as that for \mathbf{f}_0 in Eq. (1), $p(\mathbf{f}_0 | \mathbf{u}_0)$ is conditionally Gaussian and $\mathbf{J}_{\mathbf{a}} = \prod_{k=0}^{K-1} \left| \frac{\partial \mathbb{G}_{\theta_k}(\mathbf{a})}{\partial \mathbf{a}} \right|^{-1}$ is the (diagonal) Jacobian of the transformation of the stochastic process \mathbf{a} . Rios (2020) formally proves that stochastic processes transformed by such marginal flows induce valid stochastic processes. In turn, this guarantees that the transformed sparse stochastic process is consistent—and thus a valid function prior.

One important property of the original bound proposed by Titsias (2009) is that the variational posterior implicitly cancels the conditional, as this alleviates the need for computing $\mathcal{O}(N^3)$ matrix inverses (Bauer et al., 2016). Using the same algebraic tricks, we define our approximate posterior such that *both* the conditional and the Jacobians cancel

$$q(\mathbf{f}_K, \mathbf{u}_K) = p(\mathbf{f}_K | \mathbf{u}_K) \underbrace{q(\mathbf{u}_0) \mathbf{J}_{\mathbf{u}_K}}_{=q(\mathbf{u}_K)}$$

where the $p(\mathbf{f}_K | \mathbf{u}_K)$ and $\mathbf{J}_{\mathbf{u}_K}$ are defined as before and $q(\mathbf{u}_0) = \mathcal{N}(\mathbf{u}_0 | \mathbf{m}, \mathbf{S})$ is a free form Gaussian with $\mathbf{m} \in \mathbb{R}^{M \times 1}$ and $\mathbf{S} \in \mathbb{R}^{M \times M}$. Another crucial side-effect of defining the variational posterior in this way is that it allows us to integrate out \mathbf{u}_K analytically. Following Hensman et al. (2013) we do not collapse $q(\mathbf{u}_0)$ in order for stochastic Variational Inference to scale, resulting in the following ELBO:

$$\mathcal{L}(\mathbf{Y}) = \mathbb{E}_{q(\mathbf{f}_K, \mathbf{u}_K)} \left[\log \frac{p(\mathbf{Y} | \mathbf{f}_K) \cancel{p(\mathbf{f}_K | \mathbf{u}_K)} \cancel{p(\mathbf{u}_0) \mathbf{J}_{\mathbf{u}_K}}}{\cancel{p(\mathbf{f}_K | \mathbf{u}_K)} q(\mathbf{u}_0) \cancel{\mathbf{J}_{\mathbf{u}_K}}} \right]$$

which after some algebraic manipulations (see App. A) simplifies to our proposed variational lower bound:

$$\sum_{n=1}^N \mathbb{E}_{q(\mathbf{f}_{0,n})} [\log p(\mathbf{Y}_n | \mathbb{G}_{\theta}(\mathbf{f}_{0,n}))] - \text{KL}[q(\mathbf{u}_0) || p(\mathbf{u}_0)].$$

The use of marginal flows and factorizing likelihoods results in the expected log likelihood (ELL) term being decomposable across the latent variables $q(\mathbf{f}_{0,n})$ and observations \mathbf{Y}_n —making it particularly suitable for stochastic variational inference and big N (Hensman et al., 2013). The individual ELL components will generally be unavailable in closed form and computed using one-dimensional Gaussian quadrature (Hensman et al., 2015).

4.2 A Sparsification of Previous Models

Note that our approximation directly provides a new sparse variational inference algorithm for the models proposed by Wilson and Ghahramani (2010) and Wauthier and Jordan (2010). In methodological terms, it is a direct generalization of Hensman et al. (2013) (for $\mathbb{G}_{\theta} \neq \mathbf{I}$). Crucially, this means that while our model allows for substantially more expressive function priors, it inherits the computational efficiency of the standard variational GP model.

While we focus mainly on prior transformations, our variational approximation also allows for transformations of the likelihood. Following Snelson et al. (2003) the transformed likelihood is given by:

$$p(\mathbf{Y} | \mathbb{T}, \mathbf{f}_K) = p(\mathbb{T}(\mathbf{Y}) | \mathbf{f}_K) \mathbf{J}_{\mathbf{Y}_K}.$$

where the Jacobian term does not depend on \mathbf{f}_0 . Substituting this into our bound results in

$$\tilde{\mathcal{L}} = \mathcal{L}(\mathbb{T}(\mathbf{Y})) - \log \mathbf{J}_{\mathbf{Y}_K}.$$

Setting $\mathbb{G}_{\theta} = \mathbf{I}$, this constitutes the first sparse variational approximation to the work of Snelson et al. (2003) and Rios and Tobar (2019). Unlike previous inference schemes available for these models, this makes them applicable to large-scale applications through sparse GPs and mini-batching. We demonstrate this contribution in our experiments, and call this new inference scheme variational Warped GP (v-WGP).

4.3 Bayesian Input-dependent Flows

For input-dependent flows whose parameters have Bayesian priors, we specify priors and variational posteriors that are independent of \mathbf{f}_K . For the case of the input-dependent flow being a NN, this means that

$$\begin{aligned} p(\mathbf{W}, \mathbf{f}_K) &= p_{\lambda}(\mathbf{W}) p(\mathbf{f}_K) \\ q(\mathbf{f}_K, \mathbf{W}) &= q(\mathbf{W}) q(\mathbf{f}_K) \end{aligned}$$

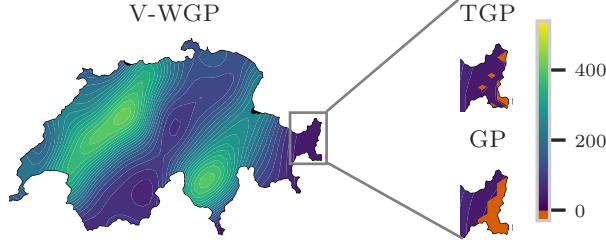


Figure 4: Spatial median predictions from a v-WGP, TGP and GP on the Switzerland daily rainfall dataset (units in $10 \mu m$). The v-WGP (left) is guaranteed to have non-negative predictions. The TGP and GP (right) do not and predict negative rainfall in Graubünden.

Absorbing these additional terms into the ELBO adds $-\text{KL}[q(\mathbf{W})||p(\mathbf{W})]$ to our bound. Additionally, the ELL term now requires integration over $q(\mathbf{W})$. The resulting integral could be approximated with S Monte Carlo samples $\{W_s\}_{s=1}^S$ using reparameterization, allowing unbiased gradient estimates of low variance to be computed via the approximation

$$\begin{aligned} \sum_{n=1}^N \mathbb{E}_{q(\mathbf{W})q(\mathbf{f}_{0,n})} [\log p(\mathbf{Y}_n | \mathbb{G}_{\boldsymbol{\theta}}(\mathbf{f}_{0,n}))] \approx \\ \sum_{n=1}^N \frac{1}{S} \sum_{s=1}^S \mathbb{E}_{q(\mathbf{f}_{0,n})} [\log p(\mathbf{Y}_n | \mathbb{G}_{\boldsymbol{\theta}(\mathbf{x}, \mathbf{w}_s)}(\mathbf{f}_{0,n}))]; \end{aligned}$$

In our experiments however, we instead use the Monte Carlo Dropout approximation (Gal and Ghahramani, 2016) as it is more memory-efficient and avoids well-known pathologies introduced by mean field approximate posteriors $q(\mathbf{W})$ (e.g. Turner and Sahani, 2011).

4.4 Prediction

To predict using the TGP ($\mathbb{G}_{\boldsymbol{\theta}} \neq \mathbf{I}, \mathbb{T} = \mathbf{I}$) we substitute the true posterior for its approximation $q(\mathbf{f}_K)$. The predictive distribution is then given by

$$p(\mathbf{Y}^*) = \int p(\mathbf{Y}^* | \mathbb{G}_{\boldsymbol{\theta}}(\mathbf{f}_0))q(\mathbf{f}_0) d\mathbf{f}_0.$$

For predictions, we use one-dimensional quadrature to approximate the first moment of $p(\mathbf{Y}^*)$. Confidence intervals are obtained by sampling from $p(\mathbf{Y}^*)$. Further details on predicting with Bayesian input-dependent flows and transformed likelihoods are in App. A.

5 Experiments

We first compare the TGP with likelihood-transforming methods. Second, we demonstrate the TGP’s excellent performance as a black box model by using input-dependent Bayesian flows on a range of UCI datasets

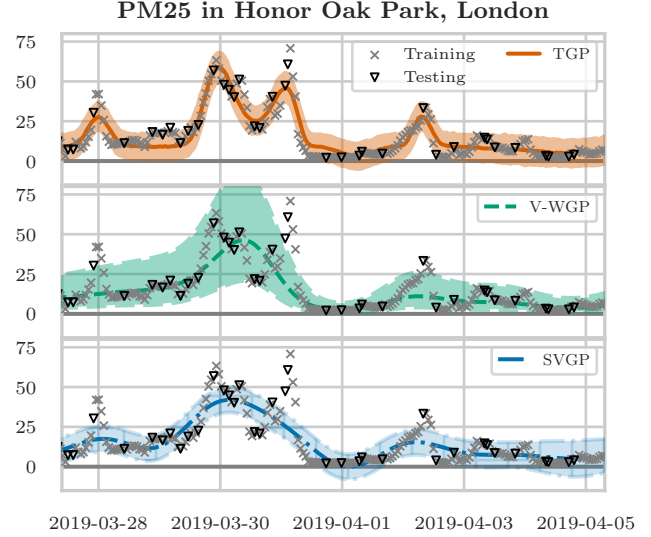


Figure 5: Model fits on PM25 with 5% of inducing points. The TGP’s added flexibility provides the best fit. **Top:** the TGP with compositional SAL and soft-plus flow. **Middle:** v-WGP with the same flow, but in reverse and applied to the likelihood. **Bottom:** SVGP.

(Lichman, 2013). All code is written in PyTorch (Paszke et al., 2019) using GPyTorch (Gardner et al., 2018). Details can be found in App. B, and all code will be publicly released.

5.1 Applications

We first study two applications to compare transformations of priors with those of likelihoods. We restrict the TGP to non-input dependent flows and we compare it against a scalable variational approximation for the Warped GP model of Snelson et al. (2003) (henceforth v-WGP) that we derive in Sec. 4.2 and the Sparse Variational GP (SVGP) of Hensman et al. (2013).

Air Quality Consider Particulate Matter of $2.5 \mu m$ size (PM25) in London (London, 2020) as depicted in Fig. 5. Measurements of PM25 are non-negative, exhibit periodic fluctuations due to vehicle traffic, and irregular peaks arising from weather conditions or traffic jams. Thus, we choose a SAL and softplus composition (SAL+SP). This makes the TGP’s latent function positive and guarantees $\mathbb{T}(\mathbf{Y}) \geq 0$ for the v-WGP.

The difference between methods is noticeable for low numbers of inducing points (see Fig. 5 & 6). As discussed in Sec. 2, the v-WGP implicitly models \mathbf{Y} with non-additive noise while the TGP transforms the prior, but models the noise additively. Hence, the TGP will attribute fluctuations to the underlying latent function, while the v-WGP is prone to absorb oscillations into the observation noise, as in Fig. 5. Unsurpris-

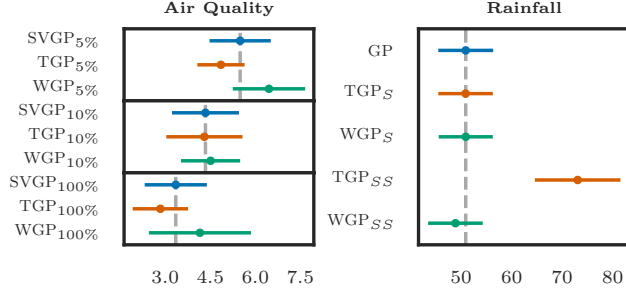


Figure 6: RMSE results (left is better) from the Air quality and Rainfall application. **Left:** Air quality experiments with 5%, 10% and 100% inducing points and a SAL plus softplus flow. The TGP consistently outperforms the GP and v-WGP because it can better fit to irregular patterns in the data. **Right:** Rainfall experiments with 100% inducing points and Softplus flows (S) versus SAL plus softplus flows (SS). When both the TGP and v-WGP use the more expressive SS flow, the v-WGP is superior, reflecting that the source of misspecification is the likelihood, not the prior.

ingly, the TGP’s fit is superior to that of the GP due to its additional flexibility. However, even though \mathbb{G}_θ is chosen so that $\mathbb{G}_\theta(\mathbf{f}_0) \geq 0$, the TGP assigns positive probability mass to PM25 being negative.

Switzerland Rainfall We also model daily rainfall in Switzerland (Dubois, 2003), see Fig. 4. As observations are non-negative, we again employ SAL+SP flows. Unlike the TGP and GP, the v-WGP does not fit the latent function to peaks in the data and guarantees positive predictions. The resulting smoother fit is desirable and explains why the v-WGP’s predictive performance in Fig. 6 outperforms that of the TGP.

5.2 Black Box results

We also highlight our model’s capability to learn arbitrary functions in a Bayesian way on a range of regression and classification problems. Throughout, the TGP uses 1- or 2-layer NNS to parameterize input-dependent flows. While the inverses of these flows would be difficult to approximate, inference for the TGP can proceed without computing the inverse transformations. This is a clear distinction to methods like the v-WGP, which relies on transforming the likelihood instead of the prior. We present results for the negative log likelihood (NLL) as they are representative for the overall findings and defer RMSE values and accuracy metrics to App. B together with details on choosing flows and NN architectures. For all plots, subscripts denote the number of inducing points used.

Bayesian Regularization First, we investigate the effect of Bayesian marginalization of the input-

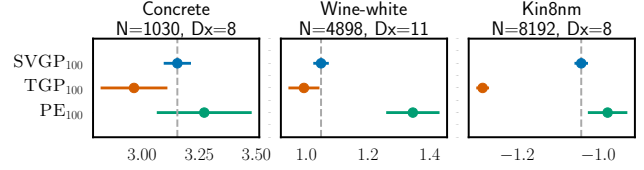


Figure 7: Comparing NLL (left is better) for a standard SVGP with an input-dependent flow indexed by a NN when the NN is estimated with a Point Estimate (PE) or integrated out in a Bayesian fashion as in the TGP

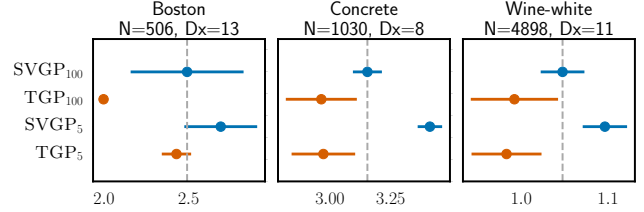


Figure 8: Comparing NLL (left is better) for some medium-sized regressions with 5 and 100 inducing points. Remaining data sets in App. B.

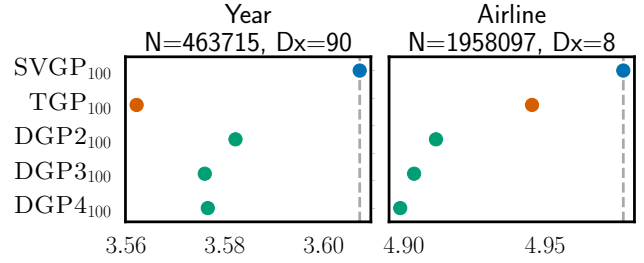


Figure 9: Comparing NLL across 2 large data sets.

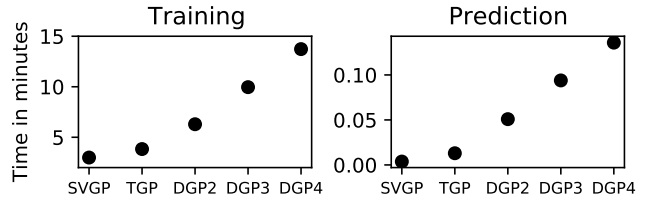


Figure 10: Average clock times for 100 runs with 1200 epochs on **energy**. Predictions use 100 samples from the posterior. The variance of training and prediction repetitions is negligible ($< 10^{-5}$).

dependent flows. In particular, we use a NN to induce input-dependence for the flow and compare the results obtained by using a point estimate via standard dropout (Srivastava et al., 2014) versus those obtained with approximate Bayesian marginalization via Monte Carlo Dropout (Gal and Ghahramani, 2016). The results are depicted in Fig. 7 and demonstrate that preventing the NN from overfitting with a Bayesian treatment yields a significant performance boost.

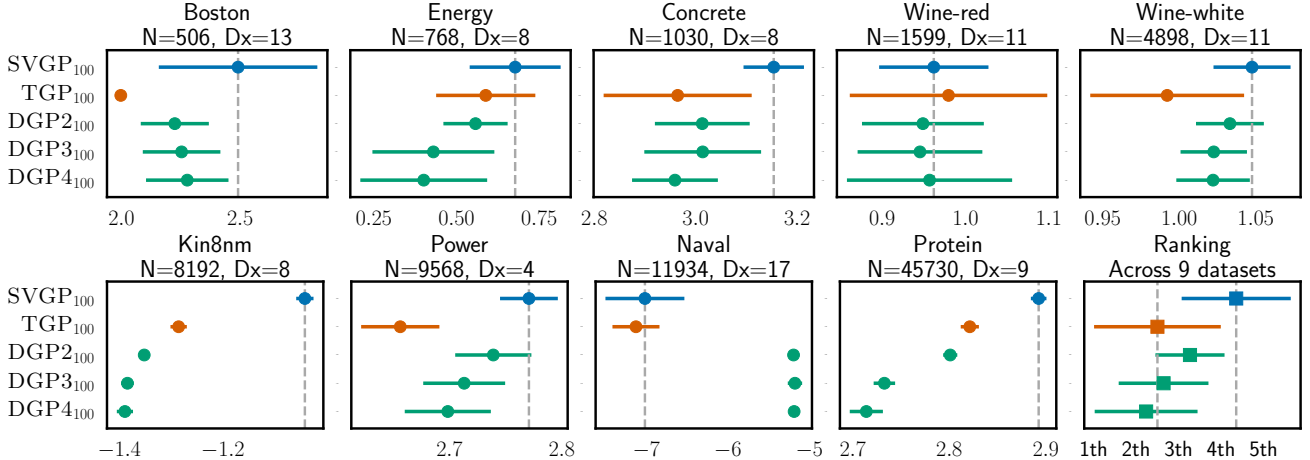


Figure 11: Comparing NLL (left is better) across 9 data sets. **Bottom rightmost panel:** Ranking of the methods across all 9 data sets and repetitions shows that the TGP performs as well as a 3- or 4-layer DGP.

Medium Scale Regression We compare TGPs, SVGPs and DGPs with 2, 3, 4 layers on a range of medium-sized data sets. For D_x denoting the dimension of \mathbf{X} , each DGP layer has at least $\min(D_x, 16)$ GP’s per layer, and we set kernel parameters and perform inference as in Salimbeni and Deisenroth (2017). Results over 10 training:test (90:10) splits are shown in Fig. 11. They demonstrate that the TGP clearly outperforms the GP and, on 4/9 datasets, the TGP even manages to outperform the 4-layer DGP. When ranking the results, this implies an overall performance comparable to that of a 3-layer DGP (see the rightmost bottom plot in Fig. 11).

Large Scale Regression We also benchmark the TGP on two large scale regression datasets. The **Year** has 0.5M, and the **airline** around 2M training data points. Fig. 9 shows the results and mirrors the findings for the medium-sized regressions.

Classification Unlike transformations of the likelihood, prior transformations can be used to improve performance for discrete-valued data. Fig. 12 makes this point using a range of classification problems.

Computational Cost Impressively, the TGP can match the 3-layer DGP’s performance at a fraction of the computational complexity: Even on the **energy** data set—where the DGP has only 4 GPs per layer—computation times for the 3-layer DGP are $3\times$ (training) and $10\times$ (prediction) that of the TGP (Fig. 10). This is true even though our implementation of the DGP fully exploits parallelization on a GPU cluster, while our current TGP implementation does not exploit potential parallelization across GP parameters.

Fewer Inducing Points The TGP can match or outperform standard GPs using 20 times fewer induc-

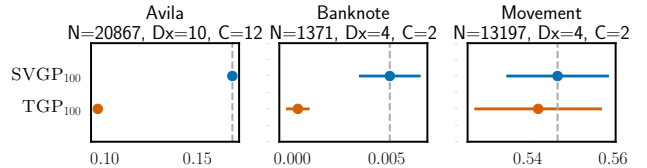


Figure 12: Comparing NLL (left is better) on three classification problems with up to $C = 12$ classes.

ing points, and we illustrate this in Fig. 8. We provide evidence on additional data sets in App. B which also shows that $\text{Cov}[q(\mathbf{f}_0)]$ does not collapse to a point mass. This implies that the Bayesian NN flow does not make the GP redundant—in fact, the TGP’s base GP is essential to our model’s quantification of uncertainty.

6 Conclusions and Future Work

We introduced Transformed Gaussian Processes (TGPs)—a new and flexible family of function priors—by enriching GPs with parameterized, invertible, input-dependent, and Bayesian transformations (aka flows). While the computational overhead of our inference scheme is comparable to that of sparse variational GP regression, its predictive performance matches that of multi-layered DGPs. The variational approximation we derived also speeds up inference in a host of other models (e.g. Wilson and Ghahramani, 2010; Wauthier and Jordan, 2010; Snelson et al., 2003) to $\mathcal{O}(NM^2 + M^3)$. Our work can be used within inter-domain inducing point approximations (Lázaro-Gredilla and Figueiras-Vidal, 2009; Dutordoir et al., 2020), to improve multitask GPs (Bonilla et al., 2007; Álvarez et al., 2012; Hamelijnck et al., 2019), density estimation (Dutordoir et al., 2018), and probabilistic dimensionality reduction (Titsias and Lawrence, 2010).

Acknowledgments

J. M. is supported by grant FPI-UPV under grant agreement No 825111 DeepHealth Project, and by the Spanish National Ministry of Education through grant RTI2018-098091-B-I00. O. H., J. K., and T. D. are funded by the Lloyd’s Register Foundation programme on Data Centric Engineering through the London Air Quality project. O. H. is funded through The Alan Turing Institute PhD fellowship programme. J. K. is funded by the EPSRC grant EP/L016710/1 as part of the Oxford-Warwick Statistics Programme (OxWaSP) and the Facebook Fellowship Programme. This work is also supported by EPSRC grant EP/T004134/1, by The Alan Turing Institute for Data Science and AI under EPSRC grant EP/N510129/1 in collaboration with the Greater London Authority, by the PRHLT Research Center and by the European Union under project Sistemas de fabricación inteligentes para la industria 4.0 – grant agreement IDIFEDER/2018/025.

References

- Bauer, M., van der Wilk, M., and Rasmussen, C. E. (2016). Understanding probabilistic sparse gaussian process approximations. In Lee, D. D., Sugiyama, M., Luxburg, U. V., Guyon, I., and Garnett, R., editors, *Advances in Neural Information Processing Systems 29*, pages 1533–1541. Curran Associates, Inc.
- Bishop, C. M. (2006). *Pattern Recognition and Machine Learning*. Springer.
- Blei, D. M., Kucukelbir, A., and McAuliffe, J. D. (2017). Variational inference: A review for statisticians. *Journal of the American Statistical Association*, 112(518):859–877.
- Bonilla, E. V., Chai, K. M. A., and Williams, C. K. I. (2007). Multi-task gaussian process prediction. In *Proceedings of the 20th International Conference on Neural Information Processing Systems*, NIPS’07, page 153–160, Red Hook, NY, USA. Curran Associates Inc.
- Box, G. E. P. and Cox, D. R. (1964). An analysis of transformations. *Journal of the Royal Statistical Society. Series B (Methodological)*, 26(2):211–252.
- Calandra, R., Peters, J., Rasmussen, C. E., and Deisenroth, M. P. (2016). Manifold gaussian processes for regression. In *2016 International Joint Conference on Neural Networks (IJCNN)*, pages 3338–3345.
- Chen, S. S. and Gopinath, R. A. (2000). Gaussianization. In *Proceedings of the 13th International Conference on Neural Information Processing Systems*, NIPS’00, page 402–408, Cambridge, MA, USA. MIT Press.
- Damianou, A. and Lawrence, N. (2013). Deep gaussian processes. In Carvalho, C. M. and Ravikumar, P., editors, *Proceedings of the Sixteenth International Conference on Artificial Intelligence and Statistics*, volume 31 of *Proceedings of Machine Learning Research*, pages 207–215, Scottsdale, Arizona, USA. PMLR.
- Dezfouli, A. and Bonilla, E. V. (2015). Scalable inference for gaussian process models with black-box likelihoods. In *Proceedings of the 28th International Conference on Neural Information Processing Systems - Volume 1*, NIPS’15, page 1414–1422, Cambridge, MA, USA. MIT Press.
- Diggle, P. and Ribeiro, P. (2007). *Model-based Geostatistics*. Springer Series in Statistics. Springer.
- Dubois, G. (2003). *Mapping radioactivity in the environment : Spatial Interpolation Comparison 97*. Office for Official Publications of the European Communities, Luxembourg.
- Dutordoir, V., Durrande, N., and Hensman, J. (2020). Sparse gaussian processes with spherical harmonic features. In *International Conference on International Conference on Machine Learning*.
- Dutordoir, V., Salimbeni, H., Hensman, J., and Deisenroth, M. (2018). Gaussian process conditional density estimation. In Bengio, S., Wallach, H., Larochelle, H., Grauman, K., Cesa-Bianchi, N., and Garnett, R., editors, *Advances in Neural Information Processing Systems 31*, pages 2385–2395. Curran Associates, Inc.
- Einstein, A. (1905). Über die von der molekularkinetischen theorie der wärme geforderte bewegung von in ruhenden flüssigkeiten suspendierten teilchen. *Annalen der physik*, 4.
- Gal, Y. and Ghahramani, Z. (2016). Dropout as a bayesian approximation: Representing model uncertainty in deep learning. In *Proceedings of the 33rd International Conference on International Conference on Machine Learning - Volume 48*, ICML’16, page 1050–1059. JMLR.org.
- Gardner, J. R., Pleiss, G., Bindel, D., Weinberger, K. Q., and Wilson, A. G. (2018). Gpytorch: Black-box matrix-matrix gaussian process inference with gpu acceleration. In *Advances in Neural Information Processing Systems*.
- Garnelo, M., Schwarz, J., Rosenbaum, D., Viola, F., Rezende, D. J., Eslami, S. M. A., and Teh, Y. W. (2018). Neural processes. In *Workshop on Theoretical Foundations and Applications of Deep Generative Models, International Conference on Machine Learning*.

- Hamelijnck, O., Damoulas, T., Wang, K., and Girolami, M. (2019). Multi-resolution multi-task gaussian processes. In *Advances in Neural Information Processing Systems*, pages 14025–14035.
- Hartmann, M. and Vanhatalo, J. (2019). Laplace approximation and natural gradient for gaussian process regression with heteroscedastic student-t model. *Statistics and Computing*, 29(4):753–773.
- Hensman, J., de G. Matthews, A. G., and Ghahramani, Z. (2015). Scalable variational gaussian process classification. In Lebanon, G. and Vishwanathan, S. V. N., editors, *AISTATS*, volume 38 of *JMLR Workshop and Conference Proceedings*. JMLR.org.
- Hensman, J., Fusi, N., and Lawrence, N. D. (2013). Gaussian processes for big data. In *Proceedings of the Twenty-Ninth Conference on Uncertainty in Artificial Intelligence*, UAI’13, page 282–290, Arlington, Virginia, USA. AUAI Press.
- Jones, M. C. and Pewsey, A. (2009). Sinh-arcsinh distributions. *Biometrika*, 96(4):761–780.
- Jylänki, P., Vanhatalo, J., and Vehtari, A. (2011). Robust gaussian process regression with a student-t likelihood. *Journal of Machine Learning Research*, 12(11).
- Kingma, D. P. and Welling, M. (2014). Auto-Encoding Variational Bayes. In *2nd International Conference on Learning Representations, ICLR 2014, Banff, AB, Canada, April 14-16, 2014, Conference Track Proceedings*.
- Knoblauch, J. (2019). Robust deep gaussian processes. *arXiv preprint arXiv:1904.02303*.
- Knoblauch, J., Jewson, J., and Damoulas, T. (2019). Generalized variational inference: Three arguments for deriving new posteriors. *arXiv preprint arXiv:1904.02063*.
- Krige, D. G. (1951). *A statistical approach to some mine valuation and allied problems on the Witwatersrand: By DG Krige*. PhD thesis, University of the Witwatersrand.
- Lázaro-Gredilla, M. (2012). Bayesian warped gaussian processes. In Pereira, F., Burges, C. J. C., Bottou, L., and Weinberger, K. Q., editors, *Advances in Neural Information Processing Systems 25*, pages 1619–1627. Curran Associates, Inc.
- Lázaro-Gredilla, M. and Figueiras-Vidal, A. (2009). Inter-domain gaussian processes for sparse inference using inducing features. In Bengio, Y., Schuurmans, D., Lafferty, J. D., Williams, C. K. I., and Culotta, A., editors, *Advances in Neural Information Processing Systems 22*, pages 1087–1095. Curran Associates, Inc.
- Lichman, M. (2013). UCI machine learning repository.
- Lin, L.-H. and Joseph, V. R. (2019). Transformation and additivity in gaussian processes. *Technometrics*, 0(0):1–11.
- London, I. C. (2020). Londonair - london air quality network (laqn). <https://www.londonair.org.uk>.
- Meng, C., Song, Y., Song, J., and Ermon, S. (2020). Gaussianization flows. volume 108 of *Proceedings of Machine Learning Research*, pages 4336–4345, Online. PMLR.
- Monterrubio-Gómez, K., Roininen, L., Wade, S., Damoulas, T., and Girolami, M. (2020). Posterior inference for sparse hierarchical non-stationary models. *Computational Statistics & Data Analysis*, page 106954.
- Murray, I., MacKay, D., and Adams, R. P. (2009). The gaussian process density sampler. In *Advances in Neural Information Processing Systems*, pages 9–16.
- Muré, J. (2018). Trans-gaussian kriging in a bayesian framework : a case study. *arXiv: Applications*.
- O’Hagan, A. (1978). Curve fitting and optimal design for prediction. *Journal of the Royal Statistical Society: Series B (Methodological)*, 40(1):1–24.
- Oliveira, V. D., Kedem, B., and Short, D. A. (1997). Bayesian prediction of transformed gaussian random fields. *Journal of the American Statistical Association*, 92(440):1422–1433.
- Opper, M. and Archambeau, C. (2009). The variational gaussian approximation revisited. *Neural Comput.*, 21(3):786–792.
- Papamakarios, G., Nalisnick, E. T., Rezende, D. J., Mohamed, S., and Lakshminarayanan, B. (2019). Normalizing flows for probabilistic modeling and inference. abs/1912.02762.
- Papamakarios, G., Pavlakou, T., and Murray, I. (2017). Masked autoregressive flow for density estimation. In Guyon, I., Luxburg, U. V., Bengio, S., Wallach, H., Fergus, R., Vishwanathan, S., and Garnett, R., editors, *Advances in Neural Information Processing Systems 30*, pages 2338–2347. Curran Associates, Inc.
- Paszke, A., Gross, S., Massa, F., Lerer, A., Bradbury, J., Chanan, G., Killeen, T., Lin, Z., Gimelshein, N., Antiga, L., Desmaison, A., Kopf, A., Yang, E., DeVito, Z., Raison, M., Tejani, A., Chilamkurthy, S., Steiner, B., Fang, L., Bai, J., and Chintala, S. (2019). Pytorch: An imperative style, high-performance deep learning library. In Wallach, H., Larochelle, H., Beygelzimer, A., d Alché-Buc, F.,

- Fox, E., and Garnett, R., editors, *Advances in Neural Information Processing Systems 32*, pages 8024–8035. Curran Associates, Inc.
- Quiñonero Candela, J. and Rasmussen, C. E. (2005). A unifying view of sparse approximate gaussian process regression. *J. Mach. Learn. Res.*, 6:1939–1959.
- Rezende, D. and Mohamed, S. (2015). Variational inference with normalizing flows. In Bach, F. and Blei, D., editors, *Proceedings of the 32nd International Conference on Machine Learning*, volume 37 of *Proceedings of Machine Learning Research*, pages 1530–1538, Lille, France. PMLR.
- Rios, G. (2020). Transport gaussian processes for regression.
- Rios, G. and Tobar, F. (2019). Compositionally-warped gaussian processes. *Neural Networks*, 118:235–246.
- Salimbeni, H. and Deisenroth, M. (2017). Doubly stochastic variational inference for deep gaussian processes. In Guyon, I., Luxburg, U. V., Bengio, S., Wallach, H., Fergus, R., Vishwanathan, S., and Garnett, R., editors, *Advances in Neural Information Processing Systems 30*, pages 4588–4599. Curran Associates, Inc.
- Sklar, A. (1959). Fonctions de répartition à n dimensions et leurs marges. *Publications de l’Institut de Statistique de l’Université de Paris*, 8:229–231.
- Snelson, E., Rasmussen, C. E., and Ghahramani, Z. (2003). Warped gaussian processes. In *Proceedings of the 16th International Conference on Neural Information Processing Systems*, NIPS’03, page 337–344, Cambridge, MA, USA. MIT Press.
- Srivastava, N., Hinton, G., Krizhevsky, A., Sutskever, I., and Salakhutdinov, R. (2014). Dropout: A simple way to prevent neural networks from overfitting. *J. Mach. Learn. Res.*, 15(1):1929–1958.
- Titsias, M. (2009). Variational learning of inducing variables in sparse gaussian processes. volume 5 of *Proceedings of Machine Learning Research*, pages 567–574, Hilton Clearwater Beach Resort, Clearwater Beach, Florida USA. PMLR.
- Titsias, M. and Lawrence, N. D. (2010). Bayesian gaussian process latent variable model. volume 9 of *Proceedings of Machine Learning Research*, pages 844–851, Chia Laguna Resort, Sardinia, Italy. JMLR Workshop and Conference Proceedings.
- Tsai, A. C., Liou, M., Simak, M., and Cheng, P. E. (2017). On hyperbolic transformations to normality. *Computational Statistics & Data Analysis*, 115:250–266.
- Tukey, J. W. (1977). *Exploratory Data Analysis*. Addison-Wesley.
- Turner, R. E. and Sahani, M. (2011). *Two problems with variational expectation maximisation for time series models*, page 104–124. Cambridge University Press.
- Uhlenbeck, G. E. and Ornstein, L. S. (1930). On the theory of the brownian motion. *Physical review*, 36(5):823.
- Ustyuzhaninov, I., Kazlauskaitė, I., Kaiser, M., Bodin, E., Campbell, N., and Henrik Ek, C. (2020). Compositional uncertainty in deep gaussian processes. volume 124 of *Proceedings of Machine Learning Research*, pages 480–489, Virtual. PMLR.
- Wauthier, F. L. and Jordan, M. I. (2010). Heavy-tailed process priors for selective shrinkage. In Lafferty, J. D., Williams, C. K. I., Shawe-Taylor, J., Zemel, R. S., and Culotta, A., editors, *Advances in Neural Information Processing Systems 23*, pages 2406–2414. Curran Associates, Inc.
- Williams, C. K. and Rasmussen, C. E. (1996). Gaussian processes for regression. In *Advances in neural information processing systems*, pages 514–520.
- Williams, C. K. I. and Seeger, M. (2001). Using the nyström method to speed up kernel machines. In Leen, T. K., Dietterich, T. G., and Tresp, V., editors, *Advances in Neural Information Processing Systems 13*, pages 682–688. MIT Press.
- Wilson, A. G. and Ghahramani, Z. (2010). Copula processes. In Lafferty, J. D., Williams, C. K. I., Shawe-Taylor, J., Zemel, R. S., and Culotta, A., editors, *Advances in Neural Information Processing Systems 23*, pages 2460–2468. Curran Associates, Inc.
- Wilson, A. G., Hu, Z., Salakhutdinov, R., and Xing, E. P. (2016). Deep kernel learning. volume 51 of *Proceedings of Machine Learning Research*, pages 370–378, Cadiz, Spain. PMLR.
- Álvarez, M. A., Rosasco, L., and Lawrence, N. D. (2012). Kernels for vector-valued functions: A review. *Foundations and Trends in Machine Learning*, 4(3):195–266.

Appendix for ‘Transforming Gaussian Processes With Normalizing Flows’

Contents

A Mathematical Appendix	13
A.1 Definitions and Notation	13
A.2 Variational Lower Bound Derivation	14
A.2.1 Sparse Prior	14
A.2.2 Approximate posterior	14
A.2.3 ELBO	15
A.2.4 KL divergence	15
A.2.5 ELL with Marginal Flows	15
A.2.6 ELL with Non Marginal Flows	16
A.2.7 Computing the marginal distribution	17
A.3 Bayesian Input Dependent Flows	17
A.4 Predictions	18
A.4.1 Predicting with V-WGP	18
A.5 Other Computational Aspects	18
B Additional Details on Experiments	20
B.1 Description of Flows	20
B.2 Initializing Flows from Data	20
B.3 Initializing Flows approximately to Identity	21
B.4 Initialization of Input dependent flows	21
B.5 Real World Experiments	21
B.5.1 Air Quality	21
B.5.2 Rainfall	21
B.5.3 Table of results in figures in main paper	22
B.6 Black Box Results	22
B.6.1 Regression	23
B.6.2 Classification	28
B.7 Bayesian Flows	29
B.7.1 Uncertainty in the Warping Function	29
B.7.2 Uncertainty handled by the GP	30

A Mathematical Appendix

In this appendix we provide all the mathematical details and derivations of the model presented in the main paper, plus some additional insights. We start with some definitions that will be used during the appendix. Then we move on the derivation of the ELBO and how we make predictions. The section is ended by strengthening the computational advantages implied by our definition. In order to highlight the role of each of the elements involved in our derivations, we provide a pictorial representation of our model in figure Fig. 13.

A.1 Definitions and Notation

1. We first define some general notation. The finite subset of observations $\{\mathbf{X}^{(n)}\}_{n=1}^N$ and inducing points $\{\mathbf{Z}^{(m)}\}_{m=1}^M$ from our stochastic process are stacked into matrices \mathbf{X} and \mathbf{Z} respectively. The corresponding function evaluations are stacked into vectors \mathbf{f} and \mathbf{u} . We denote with \mathbf{f}_0 and \mathbf{f}_K to the function evaluations before and after applying the transformation \mathbb{G}_θ . We denote specific locations n or samples s with additional subscripts e.g. $\mathbf{f}_{0,n,s}$.

2. Given an invertible transformation \mathbb{G} , and the distribution $p(\mathbf{f}_K)$ induced by transforming samples from a base distribution $p(\mathbf{f}_0)$, then it holds that expectations of any function $h()$ under $p(\mathbf{f}_K)$ can be computed by integrating w.r.t the base distribution $p(\mathbf{f}_0)$. This is formally known as *probability under change of measure*. However throughout the document we will follow Rezende and Mohamed (2015) and refer to it as *LOTUS rule*. Formally, the above statement implies:

$$\mathbb{E}_{p(\mathbf{f}_K)}[h(\mathbf{f}_K)] = \mathbb{E}_{p(\mathbf{f}_0)}[h(\mathbb{G}_\theta(\mathbf{f}_0))] \quad (4)$$

3. For any transformation \mathbb{G} that induces a valid stochastic process, see Rios (2020) for examples, it holds that the probability distribution at any finite subset of locations \mathbf{X} and \mathbf{Z} is given by:

$$p(\mathbf{f}_K, \mathbf{u}_K) = p(\mathbf{f}_0, \mathbf{u}_0 | \mathbf{X}, \mathbf{Z}) \prod_{k=0}^{K-1} \underbrace{\left| \frac{\partial \mathbb{G}_\theta(\mathbf{f}_k)}{\partial \mathbf{f}_k} \quad \frac{\partial \mathbb{G}_\theta(\mathbf{f}_k)}{\partial \mathbf{u}_k} \right|}_{\mathbf{J}_{\mathbf{f}_K, \mathbf{u}_K}} \quad (5)$$

Where each element $\frac{\partial \mathbb{G}_\theta(\mathbf{f}_k)}{\partial \mathbf{f}_k}$ is itself the Jacobian of the transformation of function evaluations at \mathbf{X} . By noting that the determinant of a block diagonal matrix can be computed as:

$$\det \begin{pmatrix} A & B \\ C & D \end{pmatrix} = \det(A - BD^{-1}C) \det(D) \quad (6)$$

We can factorize the joint distribution $p(\mathbf{f}_K, \mathbf{u}_K)$ as follows:

$$\begin{aligned} p(\mathbf{f}_K, \mathbf{u}_K) &= p(\mathbf{f}_K | \mathbf{u}_K) p(\mathbf{u}_K) \\ p(\mathbf{f}_K | \mathbf{u}_K) &= p(\mathbf{f}_0 | \mathbf{u}_0) \prod_{k=0}^{K-1} \left[\underbrace{\frac{\partial \mathbb{G}_\theta(\mathbf{f}_k)}{\partial \mathbf{f}_k}}_{\mathbf{J}_{\mathbf{f}_K}} - \underbrace{\frac{\partial \mathbb{G}_\theta(\mathbf{f}_k)}{\partial \mathbf{u}_k}}_{\mathbf{J}_{\mathbf{f}_K | \mathbf{u}_K}} \left(\underbrace{\frac{\partial \mathbb{G}_\theta(\mathbf{u}_k)}{\partial \mathbf{u}_k}}_{\mathbf{J}_{\mathbf{u}_K}} \right)^{-1} \underbrace{\frac{\partial \mathbb{G}_\theta(\mathbf{u}_k)}{\partial \mathbf{f}_k}}_{\mathbf{J}_{\mathbf{u}_K | \mathbf{f}_K}} \right] \\ p(\mathbf{u}_K) &= \prod_{k=0}^{K-1} \left| \frac{\partial \mathbb{G}_\theta(\mathbf{u}_k)}{\partial \mathbf{u}_k} \right| \end{aligned}$$

where we make use of $p(\mathbf{f}_K | \mathbf{u}_K) = p(\mathbf{f}_K, \mathbf{u}_K) / p(\mathbf{u}_K)$ to derive the expression for the conditional distribution. Furthermore, note that for marginal flows, B and C are evaluated to zero and we recover the distributions used throughout the inference section in the main paper:

$$\begin{aligned} p(\mathbf{f}_K, \mathbf{u}_K) &= p(\mathbf{f}_K | \mathbf{u}_K) p(\mathbf{u}_K) \\ p(\mathbf{f}_K | \mathbf{u}_K) &= p(\mathbf{f}_0 | \mathbf{u}_0) \prod_{k=0}^{K-1} \left| \frac{\partial \mathbb{G}_\theta(\mathbf{f}_k)}{\partial \mathbf{f}_k} \right| \\ p(\mathbf{u}_K) &= \prod_{k=0}^{K-1} \left| \frac{\partial \mathbb{G}_\theta(\mathbf{u}_k)}{\partial \mathbf{u}_k} \right| \end{aligned}$$

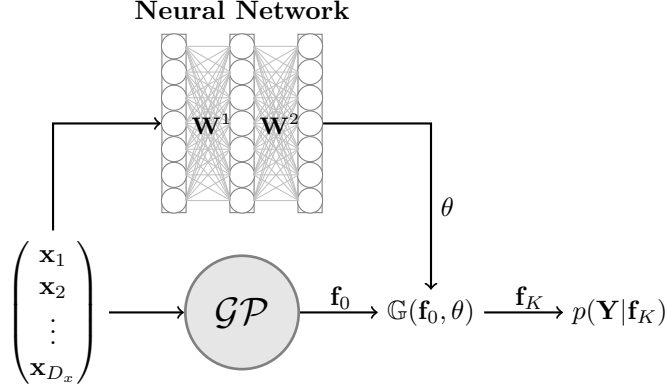


Figure 13: A pictorial representation of our general formulation that highlights the role of the Neural Network. As seen in the figure, the output of the neural network gives the parameters of the flow \mathbb{G} . We can further incorporate uncertainty into this parameters by defining a prior $p(\mathbf{W})$ over the NN parameters. See the graphical model in the main article and the details in this appendix.

where now $\left| \frac{\partial \mathbb{G}_\theta(\mathbf{f}_k)}{\partial \mathbf{f}_k} \right|$ is a diagonal matrix where the elements of the diagonal are given by $\left| \frac{\partial \mathbb{G}_\theta(\mathbf{f}_{k,n})}{\partial \mathbf{f}_{k,n}} \right|$.

A.2 Variational Lower Bound Derivation

We now provide a detailed derivation of the variational lower bound of TGP for both the marginal and non-marginal case. In order to reduce the computational cost of directly approximating the posterior at training locations \mathbf{X} (Opper and Archambeau, 2009), we make use of a sparse approximation. We begin by first defining the sparse prior and approximate variational posterior and then derive the respective lower bounds for marginal and non-marginal flows. As we will see the only difference between marginal and non marginal flows is that in the later the inducing points cannot be integrated with analytically, and so we resort to a Monte Carlo approximation.

A.2.1 Sparse Prior

For computational efficiency we follow Titsias (2009); Hensman et al. (2013) and augment the TGP prior with inducing points \mathbf{u}_K at inducing locations \mathbf{Z} . The sparse prior of TGP is defined by:

$$p(\mathbf{f}_K, \mathbf{u}_K) = p(\mathbf{f}_K | \mathbf{u}_K) p(\mathbf{u}_K) = p(\mathbf{f}_0 | \mathbf{u}_0) p(\mathbf{u}_0) \mathbf{J}_{\mathbf{f}_K, \mathbf{u}_K} \quad (7)$$

where the $p(\mathbf{u}_0)$ is a GP and the conditional $p(\mathbf{f}_0 | \mathbf{u}_0)$ is a standard Gaussian conditional:

$$\begin{aligned} p(\mathbf{u}_0) &= \mathcal{N}(\mathbf{u}_0 | 0, K_{\mathbf{Z}, \mathbf{Z}}) \\ p(\mathbf{f}_0 | \mathbf{u}_0) &= \mathcal{N}(\mathbf{f}_0 | K_{\mathbf{X}, \mathbf{Z}} K_{\mathbf{Z}, \mathbf{Z}}^{-1} \mathbf{u}_0, K_{\mathbf{X}, \mathbf{X}} - K_{\mathbf{X}, \mathbf{Z}} K_{\mathbf{Z}, \mathbf{Z}}^{-1} K_{\mathbf{Z}, \mathbf{X}}) \end{aligned} \quad (8)$$

and K is positive-semi definite kernel function. As described in the main paper, to sparsify this prior the transformation \mathbb{G} must induce a valid stochastic process. It holds that marginal flows always induce a valid stochastic process, but some care has to be taken in the definition of non-marginal flows. We refer the reader to (Rios, 2020) for examples of non-marginal transformations \mathbb{G} that transforms $p(\mathbf{f}_0)$ in a consistent way.

A.2.2 Approximate posterior

Following Titsias (2009) we define our approximate posterior such that the conditional terms cancel:

$$q(\mathbf{f}_K | \mathbf{u}_K) = p(\mathbf{f}_K | \mathbf{u}_K) q(\mathbf{u}_K) \quad (9)$$

where

$$q(\mathbf{u}_K) = \mathcal{N}(\mathbf{u}_0 | \mathbf{m}, \mathbf{S}) \mathbf{J}_{\mathbf{u}_K} \quad (10)$$

with $\mathbf{m} \in \mathbb{R}^{M \times 1}$ and $\mathbf{S} \in \mathbb{R}^{M \times M}$ being the variational parameters and $p(\mathbf{f}_K | \mathbf{u}_K)$ is given by definition 3.

A.2.3 ELBO

Following a similar derivation as Hensman et al. (2013) & Blei et al. (2017), we can arrive at the following ELBO:

$$\begin{aligned} \text{ELBO} &= \mathbb{E}_{q(\mathbf{f}_K, \mathbf{u}_K)} \left[\log \frac{\prod_n p(\mathbf{Y}_n | \mathbf{f}_{K,n}) p(\mathbf{f}_K, \mathbf{u}_K)}{q(\mathbf{f}_K, \mathbf{u}_K)} \right] \\ &= \underbrace{\sum_n \mathbb{E}_{q(\mathbf{f}_K, \mathbf{u}_K)} [\log p(\mathbf{Y}_n | \mathbf{f}_{K,n})]}_{\text{ELL}} + \underbrace{\mathbb{E}_{q(\mathbf{f}_K, \mathbf{u}_K)} \left[\log \frac{p(\mathbf{f}_K, \mathbf{u}_K)}{q(\mathbf{f}_K, \mathbf{u}_K)} \right]}_{-\text{KL}} \end{aligned} \quad (11)$$

In order to highlight the difference between using marginal and non-marginal flows, we break the derivation of the final lower bound into the KL and the expected log likelihood (ELL). As we will illustrate, only the ELL depends on the type of transformation (marginal or non) and so we first deal with the (negative) KL term.

A.2.4 KL divergence

It turns out that the KL between the prior and the approximate posterior on the transformed space \mathbf{f}_K , is given by the same KL on the original space \mathbf{f}_0 :

$$\begin{aligned} \text{KL} &= -\mathbb{E}_{q(\mathbf{f}_K, \mathbf{u}_K)} \left[\log \frac{p(\mathbf{f}_K | \mathbf{u}_K) p(\mathbf{u}_0) \mathbf{J}_{\mathbf{u}_K}}{p(\mathbf{f}_K | \mathbf{u}_K) q(\mathbf{u}_0) \mathbf{J}_{\mathbf{u}_K}} \right] \\ &= -\mathbb{E}_{q(\mathbf{u}_K)} \left[\log \frac{p(\mathbf{u}_0)}{q(\mathbf{u}_0)} \right] \\ &= \underbrace{-\mathbb{E}_{q(\mathbf{u}_0)} \left[\log \frac{p(\mathbf{u}_0)}{q(\mathbf{u}_0)} \right]}_{:= \text{KL}[q(\mathbf{u}_0) || p(\mathbf{u}_0)]} \end{aligned} \quad (12)$$

where we have first marginalized \mathbf{f}_K and then applied the LOTUS rule. By defining the approximate posterior as being transformed by the same flow as the prior it allows both the Jacobian and conditional distribution $p(\mathbf{f}_K | \mathbf{u}_K)$ to cancel. This not only alleviates costly $\mathcal{O}(N^3)$ computations coming from the KL between the conditional distributions, but also simplifies the KL to simply be between two Gaussian distributions.

A.2.5 ELL with Marginal Flows

We now derive the expected log term for the case in which \mathbb{G} is a marginal flow. To do so we first derive the form of $q(\mathbf{f}_K)$ by analytically integrating out the inducing points \mathbf{u}_K . We then marginalize \mathbf{f}_K such that the ELL term decomposes into components of $\mathbf{f}_{K,n}$ and \mathbf{Y}_n . The marginal $q(\mathbf{f}_K)$ is given by:

$$\begin{aligned} q(\mathbf{f}_K) &= \int q(\mathbf{f}_K, \mathbf{u}_K) d\mathbf{u}_K \\ &= \int p(\mathbf{f}_0 | \mathbf{u}_0) q(\mathbf{u}_0) \mathbf{J}_{\mathbf{f}_K, \mathbf{u}_K} d\mathbf{u}_K \end{aligned} \quad (13)$$

Because \mathbb{G} is a marginal flow the Jacobian matrix is diagonal and decomposes such that $\mathbf{J}_{\mathbf{f}_K, \mathbf{u}_K} = \mathbf{J}_{\mathbf{f}_K} \mathbf{J}_{\mathbf{u}_K}$. Substituting this into the above and applying LOTUS rule by recognizing this as an expectation w.r.t $q(\mathbf{u}_K)$:

$$\begin{aligned} q(\mathbf{f}_K) &= \int p(\mathbf{f}_0 | \mathbf{u}_0) q(\mathbf{u}_0) \mathbf{J}_{\mathbf{f}_K} \mathbf{J}_{\mathbf{u}_K} d\mathbf{u}_K \\ &= \mathbf{J}_{\mathbf{f}_K} \int p(\mathbf{f}_0 | \mathbf{u}_0) q(\mathbf{u}_0) d\mathbf{u}_0 \\ &= \mathbf{J}_{\mathbf{f}_K} q(\mathbf{f}_0) \end{aligned} \quad (14)$$

where $\mathbf{J}_{\mathbf{f}_K}$ does not depend on \mathbf{u}_0 and the marginal $q(\mathbf{f}_0)$ is:

$$q(\mathbf{f}_0) = \mathcal{N}(\mathbf{f}_0 | K_{\mathbf{X}, \mathbf{Z}} K_{\mathbf{Z}, \mathbf{Z}}^{-1} \mathbf{m}, K_{\mathbf{X}, \mathbf{X}} - K_{\mathbf{X}, \mathbf{Z}} K_{\mathbf{Z}, \mathbf{Z}}^{-1} [K_{\mathbf{Z}, \mathbf{Z}} + \mathbf{S}] K_{\mathbf{Z}, \mathbf{Z}}^{-1} K_{\mathbf{Z}, \mathbf{X}}) \quad (15)$$

Making use of this derivation of $q(\mathbf{f}_K)$ we can simplify the ELL term in Eq. 11:

$$\begin{aligned}
 \text{ELL} &= \sum_n^N \mathbb{E}_{q(\mathbf{f}_K, \mathbf{u}_K)} [\log p(\mathbf{Y}_n | \mathbf{f}_{K,n})] \\
 &= \sum_n \mathbb{E}_{q(\mathbf{f}_0)} [\log p(\mathbf{Y}_n | \mathbf{f}_{K,n})] \\
 &= \sum_n \mathbb{E}_{q(\mathbf{f}_{0,n})} [\log p(\mathbf{Y}_n | \mathbf{f}_{K,n})],
 \end{aligned} \tag{16}$$

where we have now applied LOTUS rule over the expectation w.r.t $q(\mathbf{f}_K)$ after integrating out \mathbf{u}_K . We finally integrate out all the elements \mathbf{f}_0 but $\mathbf{f}_{0,n}$ from our variational posterior by noting that \mathbf{Y}_n only depends on the function evaluation at position n . Thus, the ELL term now factorizes across \mathbf{Y}_n and the latent variables $\mathbf{f}_{0,n}$, as required for svi. Plugging this into the ELBO:

$$\text{ELBO} = \sum_n^N \mathbb{E}_{q(\mathbf{f}_{0,n})} [\log p(\mathbf{Y}_n | \mathbb{G}(\mathbf{f}_{0,n}))] - \mathbb{E}_{q(\mathbf{u}_0)} \left[\log \frac{p(\mathbf{u}_0)}{q(\mathbf{u}_0)} \right] \tag{17}$$

recovers the lower bound presented in the main paper.

A.2.6 ELL with Non Marginal Flows

We now present a generalization of the presented inference algorithm to include non-marginal flows where, as before, we only require that \mathbb{G} induces a valid stochastic process. The key difference between using marginal and non marginal flows is that for non-marginal flows we will not be able to, in general, analytically integrate out the inducing points \mathbf{u}_K . However, we can simply integrate them with Monte Carlo. To illustrate this fact, we proceed as in the previous section. The marginal $q(\mathbf{f}_K)$ is given by:

$$\begin{aligned}
 q(\mathbf{f}_K) &= \int q(\mathbf{f}_K, \mathbf{u}_K) d\mathbf{u}_K \\
 &= \int p(\mathbf{f}_K | \mathbf{u}_K) q(\mathbf{u}_K) d\mathbf{u}_K \\
 &= \int [\mathbf{J}_{\mathbf{f}_K} - \mathbf{J}_{\mathbf{f}_K | \mathbf{u}_K} \mathbf{J}_{\mathbf{u}_K}^{-1} \mathbf{J}_{\mathbf{u}_K | \mathbf{f}_K}] p(\mathbf{f}_0 | \mathbf{u}_0) q(\mathbf{u}_0) d\mathbf{u}_0 \\
 &= q(\mathbf{f}_0) \mathbf{J}_{\mathbf{f}_K} - \int [\mathbf{J}_{\mathbf{f}_K | \mathbf{u}_K} \mathbf{J}_{\mathbf{u}_K}^{-1} \mathbf{J}_{\mathbf{u}_K | \mathbf{f}_K}] p(\mathbf{f}_0 | \mathbf{u}_0) q(\mathbf{u}_0) d\mathbf{u}_0
 \end{aligned} \tag{18}$$

where in the last line we use LOTUS rule. Note that integrating the inducing points will be generally intractable due to the non-linearity of the flow \mathbb{G} that appears in the conditional prior $p(\mathbf{f}_K | \mathbf{u}_K)$ through the elements $\mathbf{J}_{\mathbf{f}_K | \mathbf{u}_K}$, $\mathbf{J}_{\mathbf{u}_K | \mathbf{f}_K}$ and $\mathbf{J}_{\mathbf{u}_K}$. Resorting to a Monte-Carlo approximation and simplifying the ELL term in Eq. 11:

$$\begin{aligned}
 \text{ELL} &= \sum_n \mathbb{E}_{q(\mathbf{f}_K, \mathbf{u}_K)} [\log p(\mathbf{Y}_n | \mathbf{f}_{K,n})] \\
 &= \sum_n \mathbb{E}_{q(\mathbf{f}_{K,n}, \mathbf{u}_K)} [\log p(\mathbf{Y}_n | \mathbf{f}_{K,n})] \\
 &\approx \sum_n \frac{1}{S} \sum_s [\log p(\mathbf{Y}_n | \mathbf{f}_{K,n,s})]
 \end{aligned}$$

where we follow similar steps to marginal flows, i.e. we integrate out all the elements from \mathbf{f}_K but $\mathbf{f}_{K,n}$ (see below section). The last line is the Monte-Carlo approximation where samples are obtained by the generative process defined for flow based models, i.e. *sample from the base distribution* and *warp samples with the flow*:

$$\begin{aligned}
 \mathbf{u}_{0,s} &\sim q(\mathbf{u}_0) \\
 \mathbf{f}_{0,n,s} &\sim p(\mathbf{f}_{0,n} | \mathbf{u}_{0,s}) \\
 \mathbf{f}_{K,n,s}, \mathbf{u}_{K,s} &= \mathbb{G}_\theta(\mathbf{f}_{0,n,s}, \mathbf{u}_{0,s})
 \end{aligned} \tag{19}$$

where the samples $\mathbf{u}_{K,s}$ are then discarded. Evaluation of this ELBO requires a computational complexity of $\mathcal{O}(M^3)$ and although it requires two layers of sampling (from $q(\mathbf{u}_0)$ and $p(\mathbf{f}_{0,n} | \mathbf{u}_0)$) this is similar to the

doubly stochastic framework of Salimbeni and Deisenroth (2017) where samples must be propagated through the layers of the DGP. Both sampling distributions are Gaussian and so the reparameterization trick can be used to generate low variance, unbiased gradients (Kingma and Welling, 2014). Moreover, because $p(\mathbf{f}_{0,n} | \mathbf{u}_0)$ is a univariate Gaussian sampling can be easily parallelized. No matter the choice of \mathbb{G} we have shown that we can always factorize the ELL term across \mathbf{Y} and \mathbf{f}_K making this bound applicable to stochastic variational inference (Hensman et al., 2013). This allows the ELL term to be approximated through mini-batching. Although this results in noisy gradient updates it allows TGP to be trained on millions of observations.

A.2.7 Computing the marginal distribution

We now explicitly derive the marginal $q(\mathbf{f}_{K,n})$ by integrating $\mathbf{f}_{K,a \neq n}$ from $q(\mathbf{f}_K)$ from an alternative perspective. The derivation rests on a similar assumption made by Titsias (2009) where \mathbf{u}_K is assumed to be sufficient statistics for \mathbf{f}_K . Expanding the marginal $q(\mathbf{f}_{K,n})$:

$$\begin{aligned} q(\mathbf{f}_{K,n}) &= \int q(\mathbf{f}_{K,n}, \mathbf{f}_{K,a}) d\mathbf{f}_{K,a} \\ &= \int p(\mathbf{f}_{K,n}, \mathbf{f}_{K,a} | \mathbf{u}_K) q(\mathbf{u}_K) d\mathbf{f}_{K,a} d\mathbf{u}_K \\ &= \int p(\mathbf{f}_{K,n} | \mathbf{u}_K, \mathbf{f}_{K,a}) p(\mathbf{f}_{K,a} | \mathbf{u}_K) q(\mathbf{u}_K) d\mathbf{f}_{K,a} d\mathbf{u}_K \\ &= \int p(\mathbf{f}_{K,n} | \mathbf{u}_K) q(\mathbf{u}_K) d\mathbf{u}_K \end{aligned} \tag{20}$$

For marginal flows this integration can be done analytically but for non-marginal flows we resort to Monte-Carlo approximations. The important point here is that no matter the form of \mathbb{G} we just need the finite dimensional distributions at \mathbf{Z} and $\mathbf{X}^{(n)}$ to evaluate the lower bound.

A.3 Bayesian Input Dependent Flows

To finish with the mathematical derivations that complete the full specification of our variational posterior, we describe the necessary steps for marginal Bayesian input dependent flows. The core idea is that the parameters of the flows that apply on each of the function evaluations $\mathbf{f}_{0,n}$ at each index $\mathbf{X}^{(n)}$ of the stochastic process, depend directly on the index $\mathbf{X}^{(n)}$ – rather than being shared across them. Note that as the flow still applies over each of the function evaluations $\mathbf{f}_{0,n}$ independently, then our input dependent flows correspond to an input dependent marginal flow. For arbitrary flows, one has to make sure that the necessary conditions are satisfied when the flow is made input dependent. Hence this subsection just illustrates the derivation of the ELBO within the derivation done for marginal flows.

To do so, we assume independence between the stochastic process and the parameters of the Neural Network both on the prior and the posterior:

$$\begin{aligned} p(\mathbf{f}_K, \mathbf{u}_K, \mathbf{W}) &= p(\mathbf{f}_K | \mathbf{u}_K) p(\mathbf{u}_K) p(\mathbf{W}) \\ q(\mathbf{f}_K, \mathbf{u}_K, \mathbf{W}) &= p(\mathbf{f}_K | \mathbf{u}_K) q(\mathbf{u}_K) q_\phi(\mathbf{W}) \end{aligned} \tag{21}$$

where ϕ are the variational parameters of the BNN. By plugging this into the ELBO we arrive at:

$$\begin{aligned} \text{ELBO} &= \mathbb{E}_{q(\mathbf{f}_K, \mathbf{u}_K) q(\mathbf{W})} \log \left[\frac{\prod_n p(\mathbf{Y}_n | \mathbf{f}_{K,n}) p(\mathbf{f}_K, \mathbf{u}_K) p(\mathbf{W})}{q(\mathbf{f}_K, \mathbf{u}_K) q_\phi(\mathbf{W})} \right] \\ &= \mathbb{E}_{q(\mathbf{f}_0) q_\phi(\mathbf{W})} \log \left[\prod_n p(\mathbf{Y}_n | \mathbf{f}_{K,n}) \right] - \text{KL}[q(\mathbf{u}_0) || p(\mathbf{u}_0)] - \text{KL}[q_\phi(\mathbf{W}) || p(\mathbf{W})] \\ &= \sum_n \mathbb{E}_{q(\mathbf{f}_0) q_\phi(\mathbf{W})} \log [p(\mathbf{Y}_n | \mathbb{G}_{\theta(\mathbf{x}, \mathbf{W})}(\mathbf{f}_{0,n}))] - \text{KL}[q(\mathbf{u}_0) || p(\mathbf{u}_0)] - \text{KL}[q_\phi(\mathbf{W}) || p(\mathbf{W})] \\ &\approx \sum_n \frac{1}{S} \sum_s \mathbb{E}_{q(\mathbf{f}_{0,n})} \log [p(\mathbf{Y}_n | \mathbb{G}_{\theta(\mathbf{x}, \mathbf{W}_s)}(\mathbf{f}_{0,n}))] - \text{KL}[q(\mathbf{u}_0) || p(\mathbf{u}_0)] - \text{KL}[q_\phi(\mathbf{W}) || p(\mathbf{W})] \end{aligned}$$

where $W_s \sim q_\phi(\mathbf{W})$. This bound has two interesting properties. First one can allow for low variance and unbiased gradients w.r.t ϕ by reparameterization (something satisfied for popular choices of $q(\mathbf{W})$ such as the mean-field Gaussian family). Second, one can account for prior miss-specification by substituting the KL for other divergences, which has been shown to improve the performance of this model (see Knoblauch et al., 2019).

In our work however we have implemented the BNN using Monte Carlo dropout (Gal and Ghahramani, 2016) as it can be more efficiently trained and also allow us to avoid some well-known problems of mean field VI such as variance under-estimation see e.g Bishop (2006). Nevertheless, our bound can be efficiently trained regardless of the specification of the variational family by using batched matrix computations.

Finally, note that computing the forward passes through the Neural Network are independent of the computation of $q(\mathbf{f}_0)$. This means that one can parallelize the computation of $q(\mathbf{f}_0)$ and $\theta(\mathbf{W}_s, \mathbf{X})$.

A.4 Predictions

To make predictions we replace the true, unknown, posterior with the variational approximation. At a test location \mathbf{X}^* , after integrating out the inducing points, we have:

$$\begin{aligned} p(\mathbf{Y}^* | \mathbf{X}^*, \mathbf{X}, \mathbf{Y}) &= \int p(\mathbf{Y}^* | \mathbf{f}_K^*) p(\mathbf{f}_K^* | \mathbf{X}, \mathbf{Y}) d\mathbf{f}_K^* \approx \\ &\approx \int p(\mathbf{Y}^* | \mathbf{f}_K^*) q(\mathbf{f}_K^*) d\mathbf{f}_K^* \\ &\approx \int p(\mathbf{Y}^* | \mathbf{f}_K^*) q(\mathbf{f}_0^*) d\mathbf{f}_0^* \end{aligned} \quad (22)$$

where we have again make use of the LOTUS rule. This integral can be computed with quadrature. Note that for arbitrary flows, one can integrate the inducing points by the same sampling procedure we have already introduced in Sec. A.2.6. For the case of Bayesian input dependent flows, we further approximate the integral using Monte Carlo:

$$\begin{aligned} p(\mathbf{Y}^* | \mathbf{X}^*, \mathbf{X}, \mathbf{Y}) &= \int p(\mathbf{Y}^* | \mathbf{f}_K^*, \theta(\mathbf{W}, \mathbf{X}^*)) p(\mathbf{f}_K^*, \mathbf{W} | \mathbf{X}, \mathbf{Y}) d\mathbf{f}_K^* \approx \\ &\approx \int p(\mathbf{Y}^* | \mathbf{f}_K^*) q(\mathbf{f}_K^*) q(\mathbf{W}) d\mathbf{f}_K^* d\mathbf{W} \\ &\approx \frac{1}{S} \sum_s \int p(\mathbf{Y}^* | \mathbf{f}_K^*, \theta(\mathbf{W}_s, \mathbf{X}^*)) q(\mathbf{f}_0^*) d\mathbf{f}_0^* \end{aligned} \quad (23)$$

where again each element of the Monte Carlo is a 1 dimensional quadrature integral. The whole process for both input and non-input dependent flows can be easily parallelized with batched operations over matrices. Confidence intervals are obtained by sampling from the approximate posterior predictive and computing the relevant quantiles. Moment estimation and predictive test log likelihood is done by one dimensional quadrature, Monte Carlo estimation, and the logsumexp trick. We provide full derivations of the necessary estimators in our GitHub implementation.

A.4.1 Predicting with V-WGP

The confidence intervals of the predictive distribution with a transformed likelihood ($\mathbb{T} \neq \mathbf{I}$) are the transformed confidence intervals of $p(\mathbb{T}(\mathbf{Y}^*))$:

$$CI(\mathbf{Y}^*) = \mathbb{T}^{-1}(CI(\mathbb{T}(\mathbf{Y}^*)))$$

Prediction with a transformed likelihood requires evaluating the inverse of \mathbb{T} which in general requires approximation such as Newton-Raphson.

A.5 Other Computational Aspects

To end this part of the appendix, we highlight and summarize some convenient computational aspects that derive from our approximation and what other modeling choices imply.

One of the most interesting properties of our model is that both training and predictions can be done without inverting \mathbb{G} – which allow us to use any expressive invertible transformation (see App. B). This contrasts with models that warp the likelihood, where either strong constraints must be placed on the kind of transformations employed so that the inverse can be computed analytically (Rios and Tobar, 2019); or the inverse has to be computed using numerical methods as Newton-Raphson (Snelson et al., 2003).

On the other hand, other choices for the variational distribution would imply an undesirable increase in the computational time. First, the definition of $q(\mathbf{u}_K)$ allows us to compute the KL in closed form, avoiding the need to resort to estimation by sampling and to compute the Jacobian of the transformation. Note that computing this Jacobian can be done in linear time for marginal flows although it will have, in general, a cubic cost (see Papamakarios et al. (2019) for a review on the key points of Normalizing Flows). Moreover, other choices of $q(\mathbf{u}_K)$ could require computation of the inverse $\mathbb{G}_\theta^{-1}(\mathbf{u}_K)$ to evaluate the density of the posterior sample under $p(\mathbf{u}_0)\mathbf{J}_{\mathbf{u}_K}$. On the other hand, not canceling $p(\mathbf{f}_K|\mathbf{u}_K)$ would also require to approximate the determinant of the transformation $\mathbf{J}_{\mathbf{f}_K}$ and the inverse \mathbb{G}_θ , with *the whole dataset* \mathbf{X} , something that cannot be done stochastically. So canceling this term is not only important to allow SVI, but also to avoid costly Jacobian/inverse computations.

Finally, the use of marginal flows and definition of the variational posterior allow us to analytically integrate out the inducing points – a very desirable property both for training and when making predictions.

B Additional Details on Experiments

B.1 Description of Flows

In this section we provide a description of the flows used throughout the experiments. We describe the ‘base’ transformations that are the building blocks to compositional and input dependent flows, see Table. 1.

Table 1: Description of Flows

Flow	Forward	Inverse	Parameters
Log	$\log(\mathbf{f}_0)$	$\exp(\mathbf{f}_K)$	—
Exp	$\exp(\mathbf{f}_0)$	$\log(\mathbf{f}_K)$	—
Softplus	$\log(\exp(\mathbf{f}_0) + 1)$	$\log(\exp(\mathbf{f}_K) - 1)$	—
Sinh	$\sinh(\mathbf{f}_0)$	$\operatorname{arcsinh}(\mathbf{f}_0)$	—
Arcsinh	$a \operatorname{arcsinh}(b(\mathbf{f}_0 + c)) + d$	$\sinh(\mathbf{f}_K)$	$a, b, c, d \in \mathbb{R}$
Affine (L)	$a + b \cdot \mathbf{f}_0$	$\frac{\mathbf{f}_K - a}{b}$	$a, b : \mathbb{R}$
Sinh-Archsinh	$\sinh(b \cdot \operatorname{arcsinh}(\mathbf{f}_0) - a)$	$\sinh(\frac{1}{b}(\operatorname{arcsinh}(\mathbf{f}_0) + a))$	$a, b : \mathbb{R}$
Boxcox	$\frac{1}{\lambda}(\operatorname{sgn}(\mathbf{f}_0) \mid \mathbf{f}_0 \mid^\lambda - 1)$	$\operatorname{sgn}(\lambda \cdot \mathbf{f}_0 + 1) \mid \lambda \cdot \mathbf{f}_0 + 1 \mid^{\frac{1}{\lambda}}$	$\lambda > 0$
Tukey	$\frac{1}{g}[\exp(g \cdot \mathbf{f}_0) - 1] \exp(\frac{h}{2} \mathbf{f}_0^2)$	—	$h \in \mathbb{R}^+, g \in \mathbb{R} : g \neq 0$
TanH	$a \tanh(b(\mathbf{f}_0 + c)) + d$	—	$a, b, c, d \in \mathbb{R}$

These flows may combined to construct compositional flows and their parameters may be input dependent. Moreover, we can create a new flow by linear combination of any of these flows, where the parameters have to be restricted so that each individual flows are strictly increasing/decreasing functions. An example could be the following:

$$\mathbf{f}_K = \sum_i^I a_i + b_i \cdot \operatorname{arcsinh}((\mathbf{f}_0 - c_i)/d_i); b_i, d_i \in \mathbb{R}^+ \forall i \quad (24)$$

Finally, as in Rios and Tobar (2019) we define SAL to be a Sinh-Archsinh flow with an Affine flow (L). We also consider compositions of flows made up directly by the inverse parametrization. For example in one of our experiments we experimented with the BoxCox+L flow and the InverseBoxCox+L flow. We provide this additional information in our GitHub.

B.2 Initializing Flows from Data

In this section we describe an initialization scheme that attempts to learn flow parameters that Gaussianize the prior. In the derivation we approximate the data as being noise-free and so in practice this may also be used for the likelihood transformations of the WGP. Ideally we would want to learn a normalizing flow $\mathbb{G}(\cdot)$ that transforms a standard Gaussian φ to the true prior $p(\mathbf{f}_0)$:

$$\varphi(\mathbb{G}^{-1}(\mathbf{f})) \frac{\partial \mathbb{G}^{-1}}{\partial \mathbf{f}} = p(\mathbf{f}_0) \quad (25)$$

In practice we do not have access to the true prior but instead observations \mathbf{Y} . By using \mathbf{Y} as approximate samples from $p(\mathbf{f}_0)$ we can then optimize \mathbb{G} to approximately satisfy Eq. 25. To optimize we directly minimize the KL divergence between $p(\mathbf{f}_0)$ and $\varphi(\mathbb{G}^{-1}(\mathbf{f})) \frac{\partial \mathbb{G}^{-1}}{\partial \mathbf{f}}$:

$$\text{KL} \left[p(\mathbf{f}_0) \parallel \varphi(\mathbb{G}^{-1}(\mathbf{f})) \frac{\partial \mathbb{G}^{-1}}{\partial \mathbf{f}} \right] = \mathbb{E}_{p(\mathbf{f}_0)} \left[\log \varphi(\mathbb{G}^{-1}(\mathbf{f})) \frac{\partial \mathbb{G}^{-1}}{\partial \mathbf{f}} \right] - \mathbb{E}_{p(\mathbf{f}_0)} [p(\mathbf{f}_0)] \quad (26)$$

The second term is constant w.r.t to the flow parameters and hence we only need to consider and optimize the first term. Because we have assumed that the \mathbf{Y} are approximate samples from the true prior we write:

$$E_{p(\mathbf{f}_0)} \left[\log \varphi(\mathbb{G}^{-1}(\mathbf{f})) \frac{\partial \mathbb{G}^{-1}}{\partial \mathbf{f}} \right] \approx \sum_{n=1}^N \log \varphi(\mathbb{G}^{-1}(\mathbf{Y}_n)) \frac{\partial \mathbb{G}^{-1}}{\partial \mathbf{Y}_n} = \sum_{n=1}^N \log \varphi(\mathbb{G}^{-1}(\mathbf{Y}_n)) \left(\frac{\partial \mathbb{G}}{\partial \mathbf{Y}_n} \right)^{-1} \quad (27)$$

and the final initialization optimization procedure is:

$$\arg \min_{\theta} \sum_{n=1}^N \log \varphi(\mathbb{G}^{-1}(\mathbf{Y}_n)) \frac{\partial \mathbb{G}^{-1}}{\partial \mathbf{Y}_n} \quad (28)$$

A similar derivation is used by Papamakarios et al. (2017) but in a different context.

B.3 Initializing Flows approximately to Identity

In this section we provide details on how we initialize flows close to identity. Many transformations can already recover identity but for those that cannot this method provides an effective and simple way to initialize them. To find these parameters we simply generate observations from the line $y = x : [x_n, y_n]_{n=1}^N$ and minimize the MSE loss of the flow mapping from x to y :

$$\arg \min_{\theta} \frac{1}{N} \sum_{n=1}^N (y_n - \mathbb{G}(x_n))^2 \quad (29)$$

B.4 Initialization of Input dependent flows

To initialize input dependent flows we first initialize standard (non-input dependent) flow parameters $\hat{\theta}$ by any of the procedures described above. Then, we turn the parameters into input dependent and initialize the NN parameters to match the values learned in the first step. This is done through stochastic gradient optimization, i.e. by first sampling a minibatch from the data distribution, and then minimize the empirical MSE loss between $\text{NN}(\mathbf{X})$ and $\hat{\theta}$.

B.5 Real World Experiments

For both real world experiments, we consider 2 different seeds, shuffle the observations and run 5-fold cross-validation across 2 different optimization schemes. The first optimization scheme optimizes both the variational and hyperparameters jointly. The second holds the likelihood noise fixed for 60% of iterations. This is to help avoid early local minimum that causes the models to underfit and explain the observations as noise.

For all models, we use RBF kernels with lengthscales initialized to 0.1, and Gaussian likelihoods with noise initialized to 1.0. We optimize the whitened variational objective using Adam optimizer with a learning rate of 0.01.

B.5.1 Air Quality

We used data from the London Air Quality Network London (2020) and we focus on site HP5 (Honor Oak Park, London) using 1 month of PM25 data (731 observations, date range 03/15/2019 - 04/15/2019). Because the observations are non-negative bounded we only consider the following positive enforcing flows: sal+softplus randomly initialized, sal+softplus initialized from data and a sal + sal + softplus initialized from data.

We shuffle observations and run 5-fold cross validation across 5%, 10% and 100% of inducing points and optimize each for a total of 10000 epochs. We compute means and standard deviations across all flows, folds and seeds. In the main paper we only present results using a sal+softplus (initialized from data) flow and we now present additional results across all these positive enforcing flows.

Additional results averaged across multiple flows

We now additionally present the results averaged across all the considered flows. The results echo the findings on the single flow experiment, that the TGP outperforms both the GP and V-WGP across the 3 levels of inducing points considered. This suggests that the results of the TGP are somewhat invariant to the choice of (positive enforcing) flows used.

B.5.2 Rainfall

The Switzerland rainfall uses data collected on the 8th of May 1986. Because all the observations are positively bounded we again use positive enforcing flows. We consider: softplus, sal+softplus (from data), sal+softplus

Figure 14: RMSE (left is better) on the Air quality dataset across 5%, 10% and 100% of inducing points.

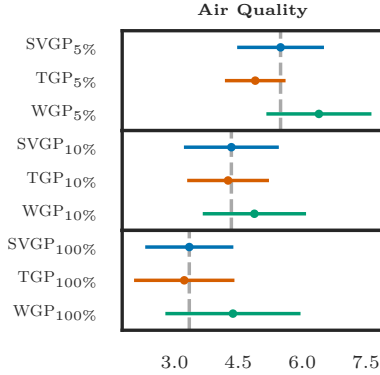


Table 2: Table of results to reproduce the left panel

Model	RMSE	Standard Deviation
GP 5	5.491	1.02
TGP 5	4.896	0.713
WGP 5	6.393	1.235
GP 10	4.335	1.115
TGP 10	4.257	0.961
WGP 10	4.876	1.214
GP 100	3.345	1.036
TGP 100	3.227	1.18
WGP 100	4.372	1.589

(from identity), sal+sal+softplus (from identity), sal+sal+softplus (from data).

We optimize for a total of 20000 epochs and compute means and standard deviations across all flows, folds and seeds.

Figure 15: RMSE (left is better) on the Rainfall experiment.

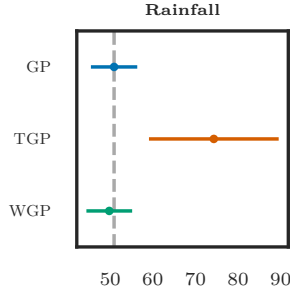


Table 3: Table of results to reproduce the left panel.

Model	RMSE	Standard Deviation
GP	50.892	5.441
TGP	74.306	15.225
WGP	49.764	5.369

B.5.3 Table of results in figures in main paper

In this section we present, for reproducibility and comparison reasons, the numerical values used to generate Fig. 6 in the main paper.

B.6 Black Box Results

In the black box experiments we explore the performance of TGP across many UCI datasets (Lichman, 2013). The performance measures are evaluated by employing random 10 fold train-test partitions and reporting average results plus standard error. This is done for all the datasets except Year and Avila (because the test partition is already provided) and Airline, where we just use a random 1 fold partition following previous works e.g (Salimbeni and Deisenroth, 2017). We perform flow selection by running each of the candidate models using random validation splits. We use one validation split on the first and second random fold partitions, except for Year and Airline where we only use one. This selection is done for 100 inducing points. The selected model is then used across all the experiments reported, including the experiments with less inducing points.

To initialize our models we follow Salimbeni and Deisenroth (2017). We use RBF kernels with parameters initialized to 2.0. The inducing points are initialized using the best of 10 KMeans runs except for Year and Airline where we just use 1 run. We use a whitened representation of inducing points and initialize the variational parameters to $\mathbf{m} = 0$ and $\mathbf{S} = 1^{-5}I$. The DGP have an additional white noise kernel added to the RBF in each hidden layer, with the noise parameter initialized to 1^{-6} . The noise parameter of the Gaussian likelihood is initialized to 0.05 for the regression experiments. For classification we use a noise free latent function and

Table 4: Table of results to generate Fig. 6 in Main paper. The left table shows results for the Air quality experiment (Left panel in Fig. 6) and the right table shows results for the rainfall experiment (Right panel in Fig. 6).

Model	RMSE	Standard Deviation
GP 5	5.491	1.02
TGP 5	4.851	0.786
WGP 5	6.451	1.207
GP 10	4.335	1.115
TGP 10	4.299	1.269
WGP 10	4.505	0.986
GP 100	3.345	1.036
TGP 100	2.833	0.923
WGP 100	4.151	1.702

Model	RMSE	Standard Deviation
GP	50.892	5.441
TGP SP	50.858	5.395
WGP SP	50.893	5.356
TGP SAL+SP	73.057	8.465
WGP SAL+SP	48.85	5.404

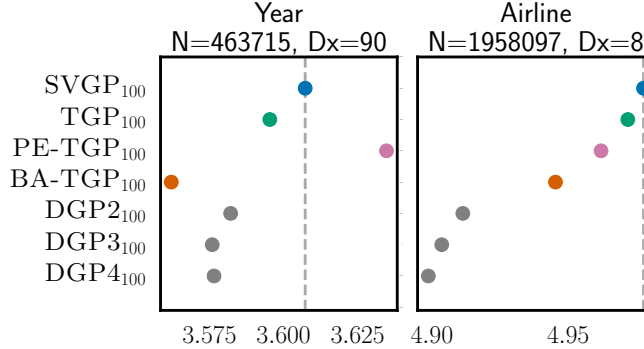
Bernoulli/Categorical likelihoods for Binary/Multiclass problems. We use probit and softmax link functions respectively. We use Adam optimizer with a learning rate of 0.01. The flow initializers are run over 2000 epochs for the identity initializer and over 2000 (rest-of-datasets) or 20 (Year-Airline) epochs for input dependent flows, to match the learned parameters in the previous initialization step. In our experiments however, we observed that the flow could be initialized with fewer epochs. We have tried a set of different combinations of flows as described in Tab. 1. This includes different flow lengths and different number of flows in the linear combinations. For input dependent flows we just tried the SAL flow with lengths 1 and 3; where dependency is encoded just in the non-linear flow (i.e the sinh-arcsinh). For these experiments we focus on exploring different architectures of the Neural Networks. We search over $\{1, 2\}$ hidden layers, $\{25, 50\}$ neurons per layer, $\{0.25, 0.5, 0.75\}$ dropout probabilities, batch normalization and ReLu and Tanh activations. We found that any of these possible combinations could work except the use of Batch Normalization. The prior over the neural network parameters is kept fixed and is introduced in the model by fixing a 1^{-5} weight decay in the optimizer ($\lambda = 1^{-5}$). In our Github we provide additional information about the model selection process and the final selected models. All of our models were optimized for 15000 epochs for all datasets except Year and Airline where we use 200 epochs. Each epoch corresponds to a full pass over the dataset. For classification we follow Hensman et al. (2015) and freeze the covariance parameters before learning everything end to end. This is done for the first 2000 epochs.

For experiments using less than 100 inducing points we use the same flow architecture selected from the validation sets and optimizer hyperparameters as the corresponding 100 inducing point experiment. The performance obtained highlights that our approach is somewhat robust to hyperparameter selection. On just one dataset we observe that this extrapolation was suboptimal and that the algorithm diverge. Those results are not reported in this appendix and correspond to 5 inducing points, input dependent flows and naval dataset. We attribute this fact to not having performed model selection for each set of inducing points specifically. On the other hand, if in any of the experiments carried out failed due to numerical errors (e.g Cholesky decomposition) we increase the standard amount of jitter added by Gpytorch from 1^{-8} to 1^{-6} . This is just needed on some train-test folds and some datasets only when using less inducing points. In general we found that our experiments were quite stable.

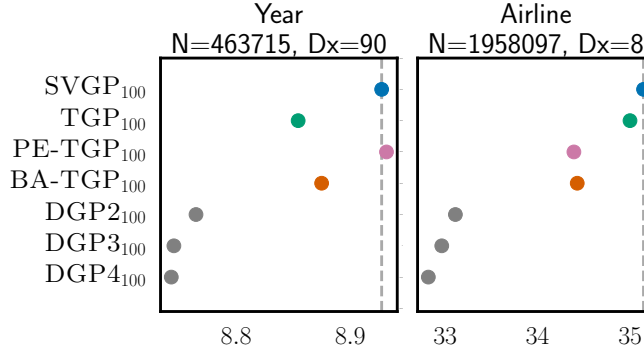
B.6.1 Regression

In this subsection we present the complete results across the regression benchmarks. This includes the NLL and RMSE for different numbers of inducing points on the following models: Sparse Variational GP (SVGP), Transformed GP with non input dependent flows (TGP), Transformed GP with point estimate input dependent flows (PE-TGP) and Transformed GP with Bayesian input dependent flows (BA-TGP). Note that PE-TGP and BA-TGP share the same input dependent architecture and learned parameters \mathbf{W} , and the only difference relies on whether we use standard Dropout (Srivastava et al., 2014) or Monte Carlo dropout (Gal and Ghahramani, 2016) to make predictions.

Large Scale Regression We report the NLL and RMSE for the Large scale regression problem in Fig. 16a and Fig. 16b. Across both datasets our model outperforms the baseline GP both in RMSE and NLL. Furthermore, the TGP also performs well, although in general is outperformed by the BA-TGP. These plots also show the regularization effect of Bayesian marginalization. In Year the RMSE and NLL is highly improved when accounting for uncertainty in the parameters. In Airline both models provide similar RMSE, but the BA-TGP provides better uncertainty quantification, reflected by improved NLL scores. In these experiments the DGP mostly outperforms TGP, PE-TGP and BA-TGP except for on the Year dataset where BA-TGP has a lower NLL, indicating better uncertainty quantification.



(a) NLL (left is better) for large scale regression datasets.



(b) RMSE (left is better) for large scale regression datasets.

Medium-Small Regression We now illustrate the results for the medium small regression in Fig. 17 (NLL) and Fig. 18 (RMSE). We show results split across decreasing number of inducing points and different models. Across all levels of inducing points, the BA-TGP model ranks the best and consistently outperforms alternative models on both NLL and RMSE showing superior point-prediction and uncertainty quantification.

On the other hand, by looking at e.g **power** dataset, and comparing RMSE and NLL, we can see how in terms of RMSE both the PE-TGP and BA-TGP perform similarly. However, there is a big difference in terms of NLL, which is an indicator of good predictive uncertainty quantification provided by introducing uncertainty in the flow parameters. We build on this observation in the final subsection of this appendix.

Moreover, a particularly interesting outcome is the performance of the models when only using 5 inducing points. We can see that in **kin8nm**, **power** and **concrete** the 5 inducing points provides a similar performance to the 100 inducing points for the BA-TGP. We show in the subsequent section that even though the Neural network is highly expressive, the base GP is necessary and not ‘ignored’ by the model. Hence we can attribute the excellent performance of BA-TGP to both the combination of the BNN and the GP.

We can also see how the standard TGP is also able to improve upon the GP in some datasets, although the improvement is minimal, clearly highlighting the necessity of input dependent flows. Also we can see in **wine-red** that while the uncertainty quantification of our model and the DGP is quite similar, we clearly outperform it in terms of pointwise predictions. The DGP consistently outperforms the TGP and SVGP w.r.t RMSE but in general the BA-TGP and PE-TGP achieve superior performance. These two observations might indicate that the proposed

model is more expressive in terms of pointwise predictions than a DGP.

Finally, note how without doing specific model selection for the less inducing points models, the parameters extrapolated from the 100 inducing points one works very well, which means that our model is somewhat robust to the selection of hyperparameter. Also by noting that all the models are trained for 15000 epochs, we show how our model has not over-fit, although being much more complex than a ‘simple’ GP.

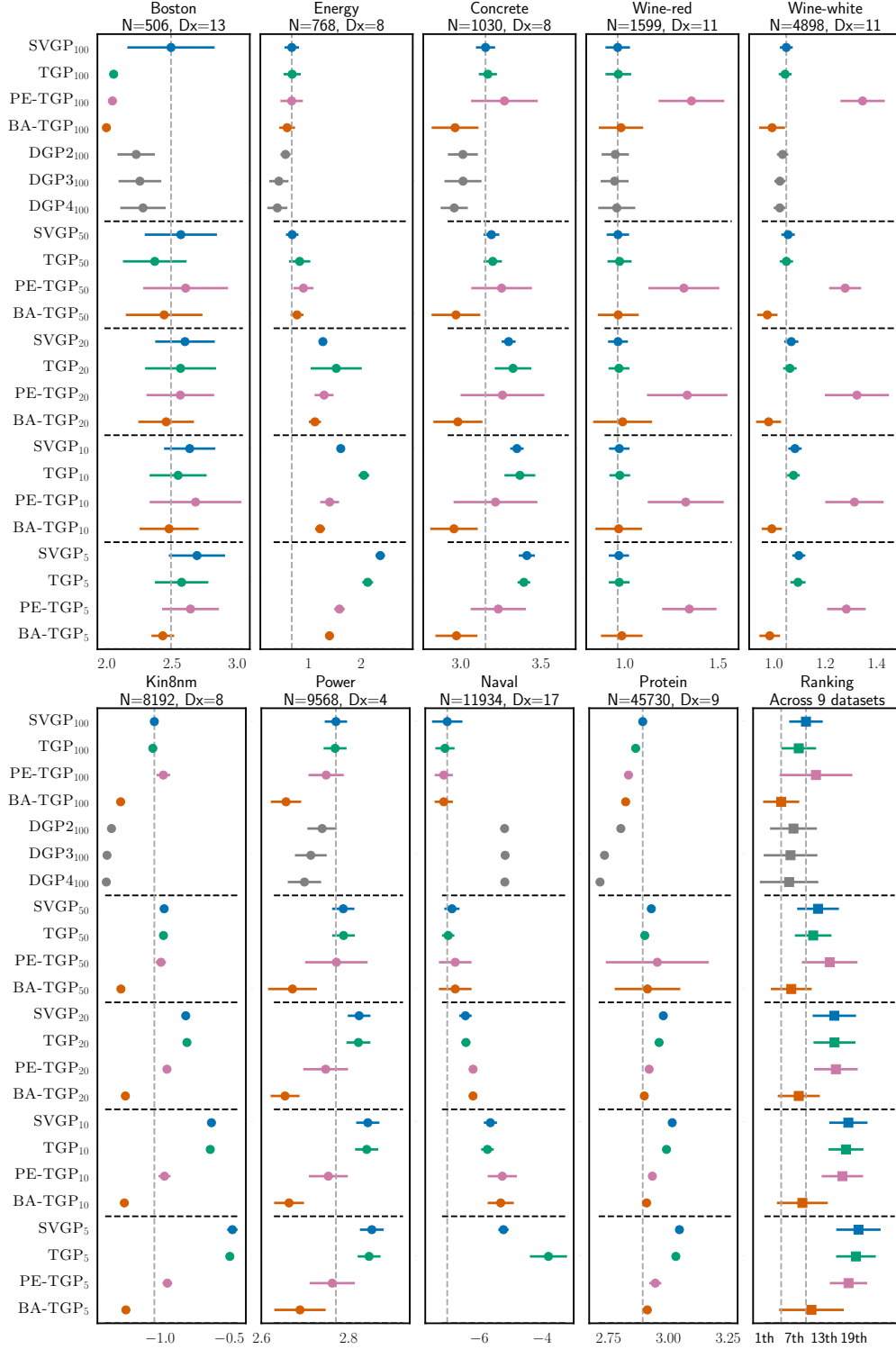


Figure 17: Comparing NLL (left is better) across 9 data sets for several number of inducing points. **Bottom right panel:** Ranking of the methods across all 9 data sets. TGP stands for non input dependent flows, PE-TGP stands for point estimate input dependent flows (Standard Dropout) and BA-TGP stands for the Bayesian input dependent flows (MC Dropout)

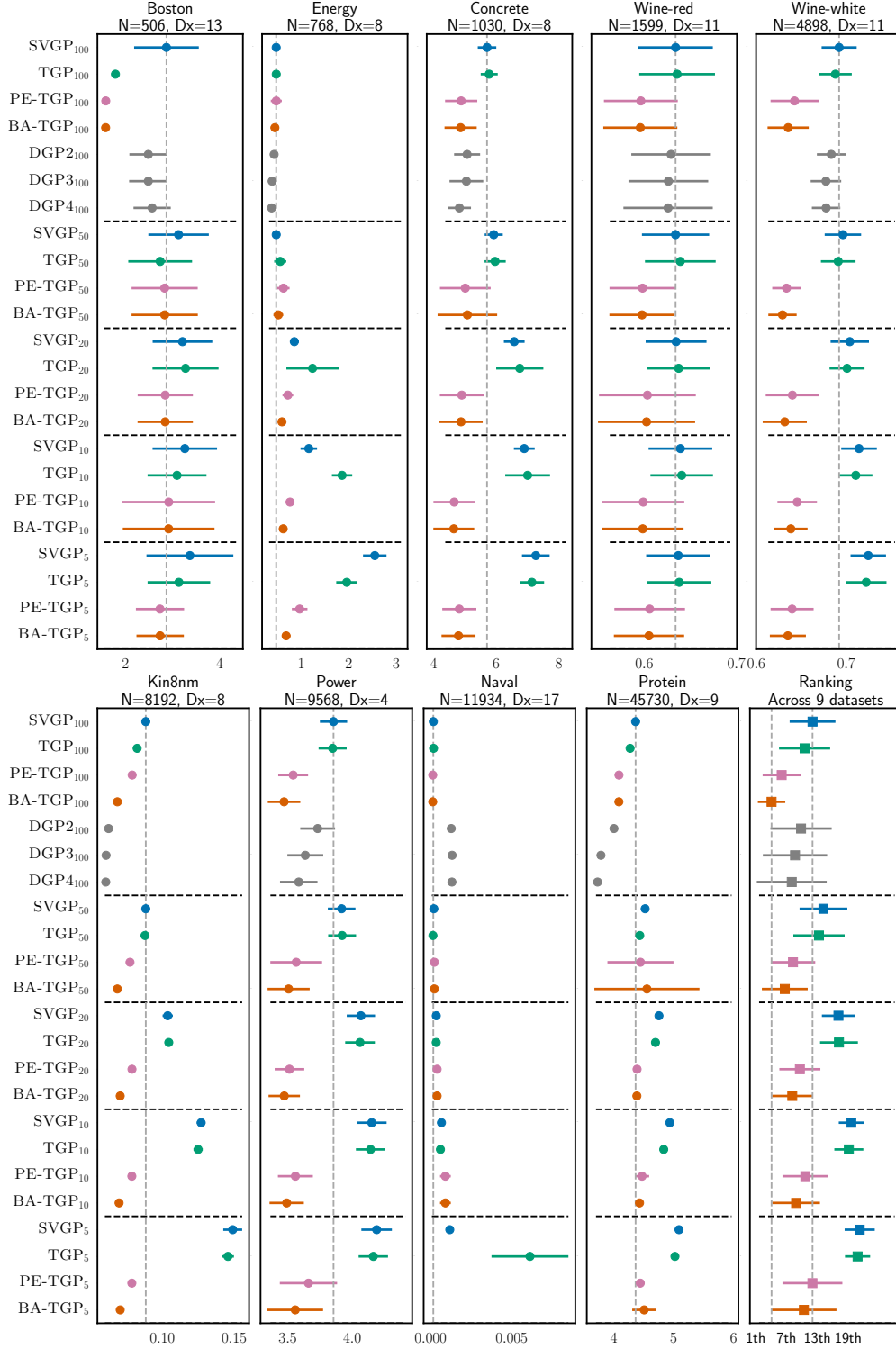


Figure 18: Comparing RMSE (left is better) across 9 data sets for several number of inducing points. **Bottom right panel:** Ranking of the methods across all 9 data sets. TGP stands for non input dependent flows, PE-TGP stands for point estimate input dependent flows (Standard Dropout) and BA-TGP stands for the Bayesian input dependent flows (MC Dropout).

B.6.2 Classification

In this section we expand on the classification experiments from the main paper by providing two additional datasets and reporting accuracy. For all the datasets we show NLL in Fig. 19a and accuracy in Fig. 19b. Across all datasets our proposed models (either through input-dependent or non-input dependent flows) outperform the SVGP, and only in **heart** does the TGP substantially outperform the input dependent models BA-TGP and PE-TGP. We highlight the big boost in accuracy provided by our models (see e.g. **avila** dataset). Surprisingly we observe that the PE-TGP performs well in classification and usually outperforms the BA-TGP. However, we have observed that sometimes the PE-TGP outputs extreme wrong values, giving a NLL of ∞ . For this same model we observe that the BA-TGP was able to remove those extreme predictions. We speculate that the model is correctly incorporating epistemic uncertainty relaxing extremely wrong assigned confidences. On the other hand, we attribute the bad performance of the BA-TGP and PE-TGP in the **heart** dataset to prior misspecification. First note that L in this case thenN is not depicted for the PE-TGP, as this is one of the cases in which many predictions were extremely wrong, yielding a ∞ NLL . We can see how the BA-TGP solves this, but due to this misspecification is unable to provide good predictions. As explained by Knoblauch et al. (2019), prior misspecification leads to a misleading quantification of uncertainty. Further, the number of training data points is small, meaning that the prior has a relatively strong influence relative to the likelihood terms. In situations like this, a badly specified prior dominates the likelihood terms and adversely affects the predictive likelihoods.

To build on this claim we note that the TGP outperforms the GP on this dataset indicating that having a more expressive prior is beneficial. This coupled with the fact that we did not tune prior $p(\mathbf{W})$ for our BNN, and that this is the only dataset in which the BA-TGP does not give a clear boost in performance, are consistent observations with the hypothesis of prior misspecification.

Finally on **banknote**, we see that all the models provide a 100% accuracy, which means that the improvement in the NLL is coming from reducing the calibration gap, as the NLL is a proper scoring rule. Our model is making the predictions extreme towards the correct class, which is a desirable property if your data distribution doesn't present overlap between classes. Note however how in this case the BA-TGP still provides uncertainty in the predictions, avoiding the extreme $\{0, 1\}$ probability assignments.

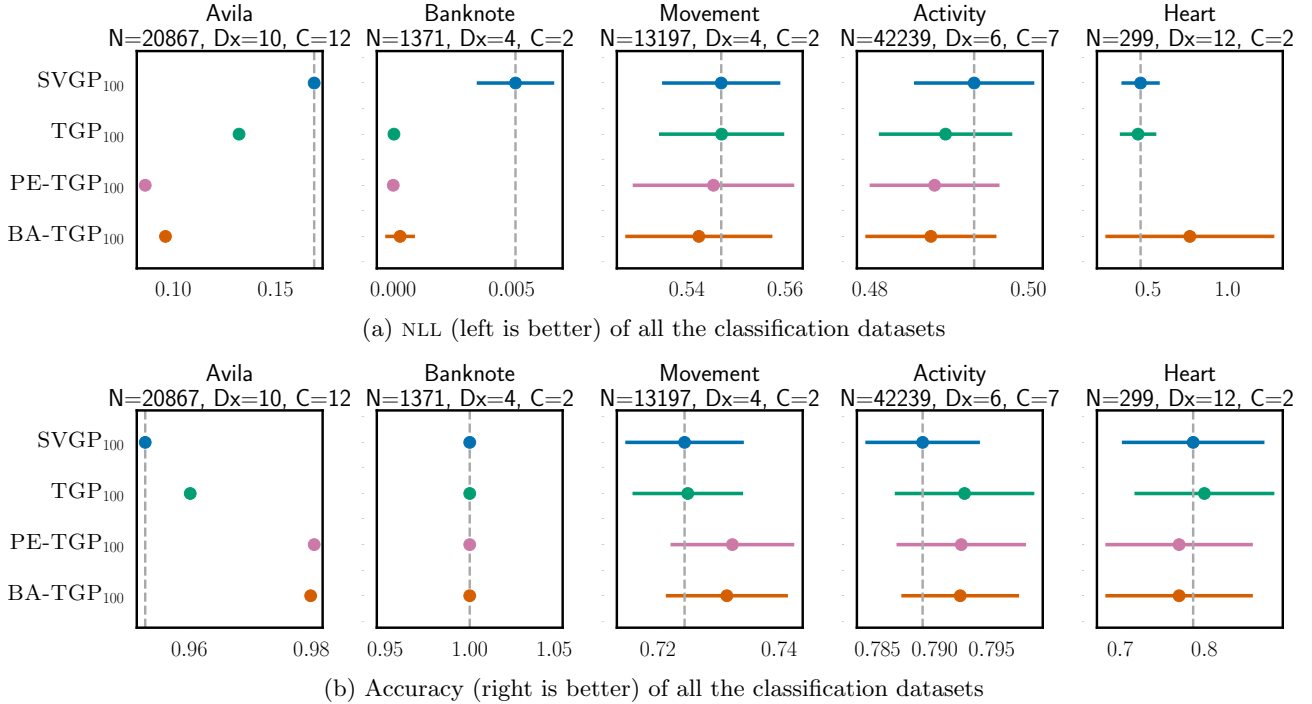


Figure 19: Results for classification datasets. TGP stands for non input dependent flows, PE-TGP stands for point estimate input dependent flows (Standard Dropout) and BA-TGP stands for the Bayesian input dependent flows (MC Dropout).

B.7 Bayesian Flows

In this subsection we provide additional information about Bayesian flows to highlight and connect with the conclusions provided in the UCI datasets section. We first show the effect of considering parameter uncertainty in the flow. We then illustrate why the whole modeling is not done by the BNN.

B.7.1 Uncertainty in the Warping Function

To illustrate the parameter uncertainty introduced by using a BNN we plot the warping function evaluated at four different training locations $\mathbf{X}^{(n)}$ for the **power** dataset. This means that we will show four different warping functions \mathbb{G} with parameters given by $\{\theta(\mathbf{W}, \mathbf{X}^{(i)})\}_{i=1}^4$. Note that the weights of the \mathbf{W} are shared and the difference in each of the parameters comes from the specific inputs \mathbf{X} . The figures show the function parameterized by the different warping functions when applied on \mathbf{f}_0 , i.e. we plot $\mathbf{f}_K = \mathbb{G}_{\theta(\mathbf{W}, \mathbf{X}^{(n)})}(\mathbf{f}_0)$. The range $\{\mathbf{f}_{0a}, \mathbf{f}_{0b}\}$ in which the flow is evaluated goes from the minimum \mathbf{Y} value in the training dataset to the maximum one. In this way we show what kind of warping function has the model learned for the output range to be regressed.

The top row in Fig. 20 shows the transformation $\mathbb{G}_{\theta(\mathbf{X}^{(n)}, \mathbf{W})}$ for the point estimate flow. The bottom row

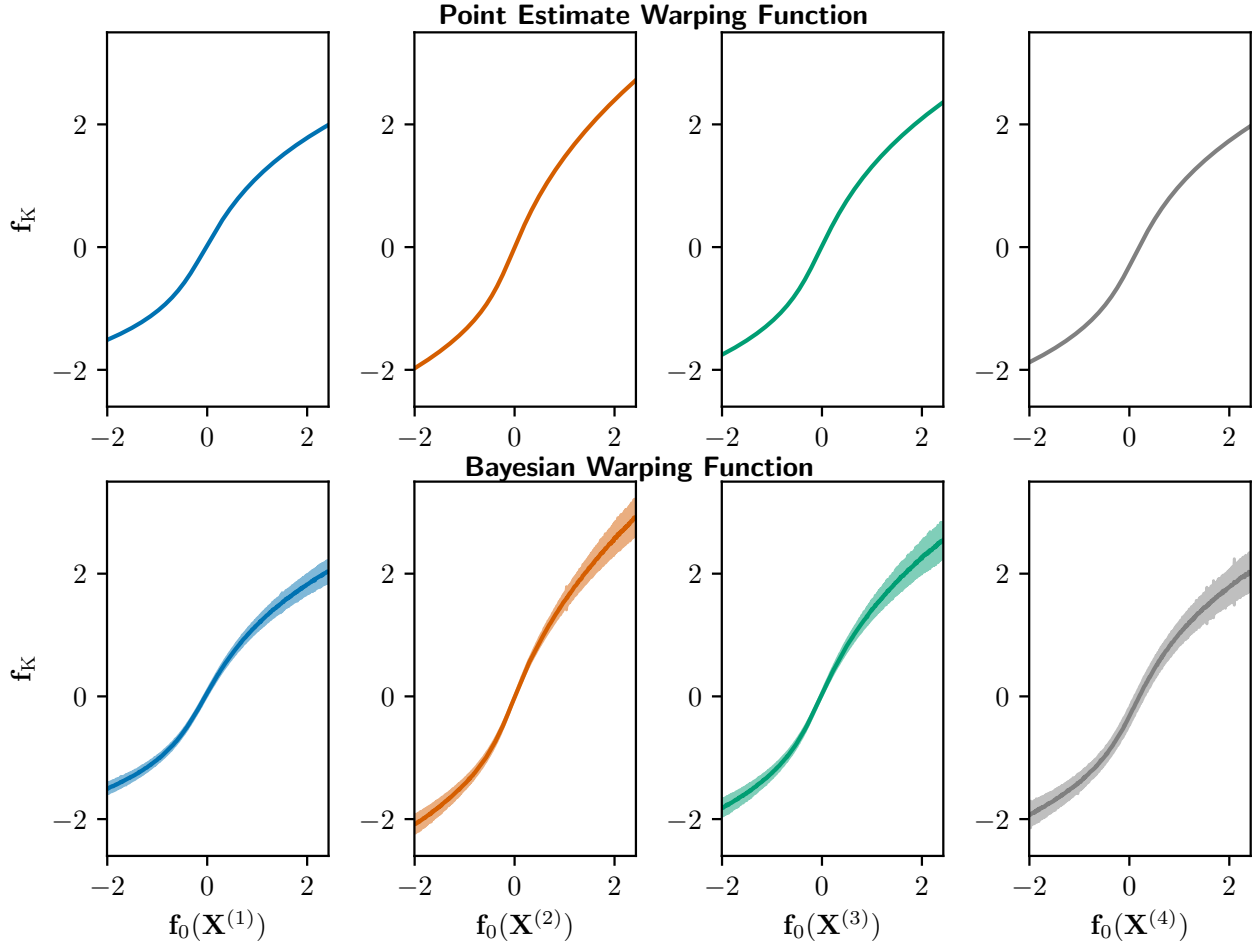


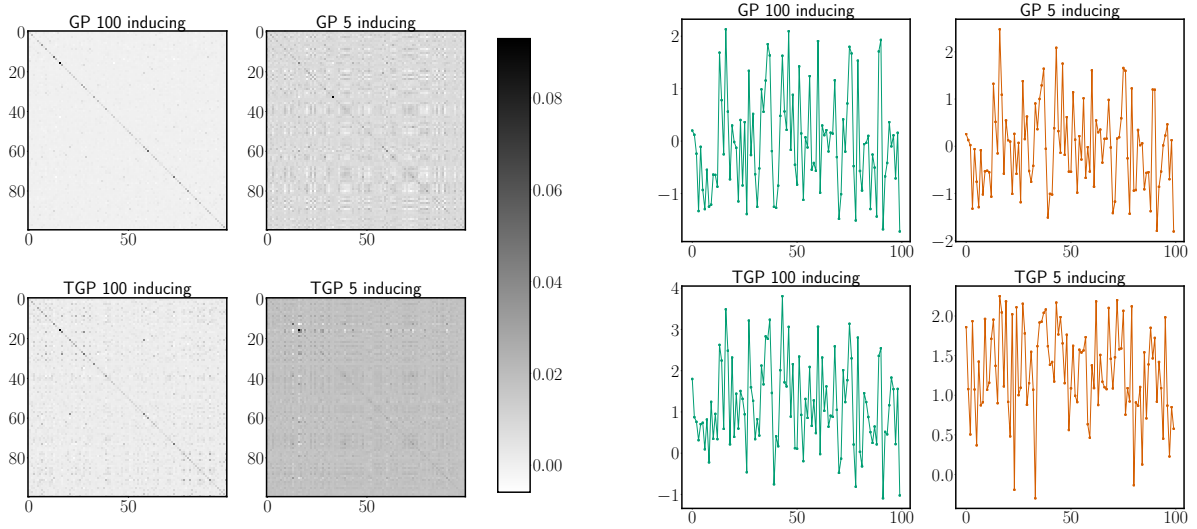
Figure 20: Example of warping functions obtained with input dependent flows for the **power** dataset. The top row shows the point estimate warping function evaluated over a range \mathbf{f}_0 , at different input locations using standard Dropout. The bottom row shows mean and standard deviation of samples from the posterior of the Bayesian flow using Monte Carlo Dropout. We can see how the model learns a different function warping depending on the input locations and how the model accounts for parameter uncertainty.

shows the mean and the standard deviation of the same flow where the parameters have been sampled from the posterior distribution. Note that the top and bottom rows use the same Neural Network parameters. The only difference is that while in the top row we compute the flow parameters with one forward pass through the Neural Network, by multiplying the activations by the 1 minus the probability of dropout p (Srivastava et al., 2014), in the bottom row we drop activations with probability p on each forward through the Neural Network (Gal and Ghahramani, 2016).

First, we can see how the model learns a different warping function for each different input $\mathbf{X}^{(n)}$, and this means that the marginal distribution at each index of our stochastic process is different. Second, we observe how the Bayesian flow incorporates parameter uncertainty. Note that both the Bayesian and point estimate flows have the same mean function; and this is the reason why the RMSE metrics reported in Fig. 18 for the **power** dataset are very similar (note that RMSE only considers the first moment of the posterior predictive). However the NLL showed in Fig. 17 is much better for the Bayesian flow, as we are incorporating epistemic uncertainty, hence being less confident in regions of function evaluations \mathbf{f}_0 where the model is uncertain. Third, note that the functions plotted for each of the training samples are simple, because the functional form is just given by a $K = 3$ input dependent flow. Hence input dependent flows are not overfitting because the functional transformation \mathbb{G} is complex, but because it is very specific for a particular point $\mathbf{X}^{(n)}$. By incorporating parameter uncertainty in the flow parameters we are considering all the possible functions parameterized by the flow’s functional \mathbb{G} , hence preventing overfitting. We can expect this regularization effect to be bigger when making the functional’s form more complex, which is something we let for future work.

B.7.2 Uncertainty handled by the GP

In the UCI experiment section we comment that sometimes the model with 5 inducing points provides similar results to the 100 inducing points models. Initially we could think that the BNN is handling all the modeling power both in terms of uncertainty quantification and regressed values. In this subsection we illustrate that this is not the case and that the modeling performance comes from a combination of the NN and the GP. Note that the uncertainty provided by the GP is combined with the uncertainty provided by the BNN.



(a) Covariance from $q(\mathbf{f}_0)$ evaluated at 100 training points (b) Mean from $q(\mathbf{f}_0)$ evaluated at 100 training points

Figure 21: This figure shows the mean and covariance from the GP variational distribution $q(\mathbf{f}_0)$ evaluated at 100 training points. As shown in the plot the covariance have not collapse to a point mass (i.e the cells would have to be completely white) and the mean also change across training points. This means that the model has not learned to just output a constant value for \mathbf{f}_0 and model everything through the Neural Network.

To do so, we pick the `concrete` dataset, which is one of the datasets in which this effect is presented. For this dataset we plot the mean and covariance of $q(\mathbf{f}_0)$ at 100 random training locations in Fig. 21. As we see in the plot, the mean and covariance from $q(\mathbf{f}_0)$ has not collapsed to a constant distribution. This means that the model has not learn to output a constant value for \mathbf{f}_0 and perform all the modelling through the input dependent $\theta(\mathbf{W}, \mathbf{X}^{(n)})$ model. Note however that understanding the specific role of the GP and the BNN in our model in terms of uncertainty quantification is something that we leave for future work.